MAPPING CROPS IN SMALLHOLDER FARM SYSTEMS FROM HIGH-SPATIAL RESOLUTION AND MULTI-TEMPORAL SATELLITE IMAGES

DICKSON NZUMBI MUKUNGA
June, 2020

SUPERVISORS:
Dr. M. Belgiu
Dr. Ir. W. Bijker

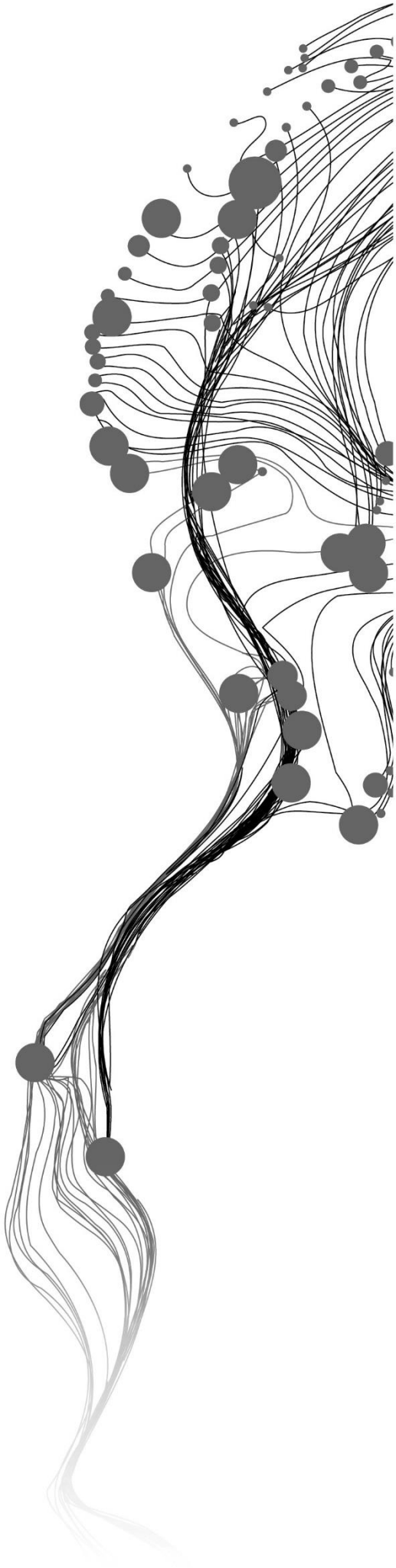

MAPPING CROPS IN SMALLHOLDER FARM SYSTEMS FROM HIGH-SPATIAL RESOLUTION AND MULTI-TEMPORAL SATELLITE IMAGES

DICKSON NZUMBI MUKUNGA

Enschede, The Netherlands, June, 2020

Thesis submitted to the Faculty of Geo-Information Science and Earth Observation of the University of Twente in partial fulfilment of the requirements for the degree of Master of Science in Geo-information Science and Earth Observation.
Specialization: Geoinformatics

SUPERVISORS:
Dr. M. Belgiu
Dr. Ir. W. Bijker

THESIS ASSESSMENT BOARD:
Prof. Dr. Ir. A, Stein (Chair)
Dr. D. Arvor (External Examiner, University of Rennes, France)

ABSTRACT

Crop mapping in smallholder farm systems has been hindered by the unavailability of high spatial resolution images. Sentinel-2 images have provided a sigh of relieve for mapping crops in smallholder farms systems due to improved spatial resolution. The emergency of PS images has presented new and attractive data product to maps crops in smallholder farm systems. Thus, the study makes use of PS images to map crop types in smallholder farms systems using TWDTW and tcDTW. The two classifiers were trained using the same data for comparison of the classification results. The comparison between the resulting overall classification accuracies from the two classifiers was tested using McNemar's test. The usability of the PS images was evaluated for spatial, spectral and temporal resolutions. The object-based classification results showed a slightly higher overall accuracy (78.08%) than pixel-based classification with an overall accuracy of 75.78%. McNemar's Chi-square test showed that the results of the two classifications were statistically significant different. Spatial suitability of PS images made use of the segmentation goodness. The spectral suitability made use NDVI generated from red edge bands of S2 images. The temporal resolution evaluation of PS images made use of the temporal nature of PS images. It was concluded that the object-based classification produced better classification overall accuracy and a more homogeneous crop type map. Additionally, from the vegetation indices generated from the red edge bands, $NDVI_{REA}1$, $NDVI_{REA}2$, and $NDVI_{REA}4$ produced better overall accuracy than classical NDVI hence can be used to improve classification accuracy. Contrary, the other vegetation indices generated from red edge bands ($NDVI_{REA}3$, NDVIren1, NDVIren2, NDVIren3, NDVIre1, NDVIre2 and NDVIre3 resulted to overall accuracy equal to or lower than the one obtained using classical NDVI hence did not improve the classification accuracy.

Keywords: PS images, NDVI time series, TWDTW, tcDTW, red edge.

ACKNOWLEDGEMENTS

Glory to Almighty God for His care, guidance and protection throughout the study in Enschede, Netherlands.

I am grateful to my supervisors; Dr. M. Belgiu and Dr. Ir. W. Bijker for their relentless advice, constructive criticism and encouragement during the research period.

I wish to extend my gratitude to the GFM staff members who have shown their support in various ways, not forgetting the lectures and codes supplied during practical classes that have proved useful in my academic journey.

I am grateful to my classmates in GFM and my friends whom we have shared light moments in the stressing times of corona.

I wish to acknowledge OKP for the grant to further my studies at ITC , University of Twente.

Special thanks to my wife; Beatrice and daughter; Abigael for their unparalleled support, encouragement and prayers throughout the study period. Lastly, I would like to share my appreciation to my parents, brothers and sisters for being a pillar to my family when I was away for the studies.

"Asanteni"

TABLE OF CONTENTS

LIST OF FIGURES

LIST OF TABLES

1. INTRODUCTION

1.1. Background information

Agriculture plays a vital role in the achievement of Sustainable Development Goals (SDGs): End poverty in all its forms everywhere and End hunger, achieve food security and improved nutrition and promote sustainable agriculture (UN News Centre, 2015). However, climate change, amongst other prevailing factors, poses a threat to the realisation of these goals. Additionally, the fast increasing population puts pressure on the existing natural resources due to increased demand for food production, with the world population estimated to be 9.8 billion by 2050 (U.N. Dept. of Economic and Social Affairs, 2017).

It is estimated that globally there are more than 475 million smallholder farms that provide food for almost a third of the world's population (Wegner and Zwart, 2011; Lowder et al., 2016). These farmers practise their agriculture in smallholder farms. Smallholder farms in this study are defined as farms less than 2 hectares(ha) Thapa (2010). Smallholder farms are usually subdivided in different fields. These farm fields may contain the same crop or different crops at the same rainy season. Persello et al. (2019) defined the agricultural(crop) field as an area of land used for agricultural purpose on which a specific crop or a crop mixture is cultivated.

Smallholder farmers remain as critical players in realisation of SGDs as they are believed to produce 70-80% of food consumed globally (Maass, 2013). Moreover, they are categorised as significant contributors to national and global food security as well as key contributors to economic growth (UNCTAD, 2015). However, these farmers are faced with challenges of low capital and erratic rainfall since they are mostly reliant on rain-fed agriculture and, hence, profoundly affected by climatic variability. Thus, availing appropriate and accurate classification and mapping methodologies for smallholder farmer systems will help in the generation of quality crop type information. The information will inform decision-makers on the formulation of policies that help boost agricultural production amongst these farmers hence reducing poverty and hunger.

Mostly, agricultural information is gathered during the national population census. Thus, the use of Earth Observation data to map smallholder crops types will come handy in providing timely, comprehensive, transparent, and accurate agricultural information (Becker-Reshef et al., 2010). Earth Observation methods are cheaper than the census method for data collection (Delrue et al., 2013) as they help to identify the crop types planted in specific regions remotely. Moreover, they help generate information on crop statistics within a particular area which is essential in planning and resource allocation such as import and export of foods from one locality to another and even at the national level (Li et al., 2007). Hence, agricultural crop mapping will help with detailed monitoring of smallholder cropping to understand food (in)security in particular areas and the nation as a whole. Besides, updated crop statistics will also help the agriculture departments to estimate the country's food production.

There has been increased use of Earth Observation in agriculture motivated by a large number of freely available satellite images such as Landsat, Moderate Resolution Imaging Spectroradiometer (MODIS) and Sentinel. Landsat images have been extensively used for agricultural land cover mapping at regional and national levels. An example of a national level mapping is a study done by Turker and Arikan (2005) employing Landsat 7 images to map crops in Turkey. On regional mapping, Xiao et al. (2005) used MODIS images to map rice paddy fields at provincial and county level in Southern China. Sentinel-1 (S1) and Sentinel-2 (S2) images provide better spatial resolution as compared to Landsat and MODIS images.

Due to their high spatial resolution, S2 data has been adopted in crop mapping in smallholder farms (Maponya et al., 2020; Lambert et al., 2018; Jin et al., 2019).

Although S2 data provides better spatial resolution than the other free sensors to map smallholder farms, heterogeneity within the smallholder farm systems requires higher spatial resolution to map. Previous studies made use of costly high-resolution satellite images such as WorldView images either to map the smallholder farms' field boundaries (Persello et al., 2019) or to identify cropped areas (McCarty et al., 2017; Neigh et al., 2018). Unfortunately, these studies cannot be replicated in other study areas because of the prohibitive costs, i.e. the costs for WorldView images are greater than $10 per km2 (McCarty et al., 2017). Therefore, cost-efficient solutions are required for identifying crop types in smallholder farms.

Thus, emergency of PS images represents a relatively new and very attractive data product for agriculture mapping due to the spatial resolution of 3 m and temporal resolution of one-two days. The short revisit time proves essential for the production of multitemporal images which have been shown to provide better accuracy than single-date images in pixel-based classification (Murthy et al., 2003; Mtibaa and Irie, 2016). The costs for accessing these images are much lower ($1.28 per km^2) than other high-resolution data products such as WorldView. PS images have been used in agriculture to map Striga weed within plantations (Mudereri et al., 2019). The authors proved that PS images achieve better results in detecting the weeds than S2 images. Despite the clear advantages of these images, they have not been exploited to their full potential for smallholder farms mapping.

Therefore this study will make use of multitemporal PS images to map crop types in smallholder farm systems using Time-weighted Dynamic Time Warping (TWDTW) (Maus et al., 2016) and time constrained Dynamic Time Warping (tcDTW) (Csillik et al., 2019).

1.2. Research Objective

The overall objective of this work is to investigate a suitable method to classify crop type in smallholder farm systems from multitemporal PlanetScope data

1.2.1. Specific objectives

1. To compare object-based and pixel-based classification approaches to map crops in smallholder farms
2. To evaluate the suitability of PlanetScope images empirically to map crops in smallholder farms

1.2.2. Research questions

1. How do pixel-based classification and object-based classification perform in terms of computational efficiency and classification accuracy in mapping crop types in smallholder farms using high spatial and temporal resolution images?
2. How does the spatial, spectral and temporal resolution of PS images enable discrimination of crop types in smallholder farmer systems in terms of classification accuracy?

2. LITERATURE REVIEW

This chapter captures relevant technical and application on smallholder crop mapping.

2.1. Multitemporal images in crop mapping

Multitemporal images have proven to provide better classification than single date images for mapping crops as they provide crops information at different phenological stages (Lunetta and Balogh, 1999; Murthy et al., 2003). Using SkySat imagery, Jain et al. (2016) were able to predict smallholder wheat yield and concluded that increased frequency of the temporal images helped in improving the accuracy of the predictions. They further noted that high spatial-temporal data could be used to map field-level yield statistics. Conrad et al. (2014), on the other hand, experimenting on the optimal number of acquisition dates to attain high classification accuracy using RapidEye images learnt that an increasing number of images does not necessarily improve classification accuracy. The authors found out that better classification results can be obtained by using an optimal number of images based on the phenological cycles of the crops to be mapped. Asgarian et al. (2016) were able to map crop types and study the dynamic agricultural fields in Iran using Landsat 8 multitemporal images. The crop type map generated proved to be important in providing agricultural information to the decision-makers on crops grown. In exploring ways to improve crop type classification accuracy, Liu et al. (2014) used synthetic and real images, to integrate low and high-resolution images. Their results showed that better crop type maps were achieved using low spatial resolution images. Further, high classification accuracy was attained when more than one images were used and when images used are from times when the crops are most distinguishable. Inglada et al. (2015) used 12 study sites to represent different global landscapes to experimented on the production of crop type maps using SPOT4, Landsat8 and RapidEye imagery. They found that the quality of crop maps were affected by the crop classes and the number of images available.
S1 & S2, Landsat8 images have been used to study the potential of multisource images in crop mapping, where the authors conclude that S1 images were weaker to identify crops than optical images Sun et al. (2019). They also noted that red-edge bands were more sensitive to vegetation than the standard bands. Meng et al. (2020) worked on establishing a temporal window which is most important for crop mapping. The authors concluded that the performance of crop mapping could be improved with the use of data from the middle and later stages of the growth cycle. Vuolo et al. (2018) assessed the impact of multitemporal data on crop type classification using S2 data. The authors found out that use of multitemporal increased the crop type classification accuracy significantly.

2.2. Crops mapping using Normalised Difference Vegetative Index (NDVI)

NDVI has been extensively used in crop mapping (Asgarian et al., 2016; Ashourloo et al., 2019; Belgiu and Csillik, 2018; Celik et al., 2015; Csillik et al., 2019; Foerster et al., 2012; Guan et al., 2016; Ouzemou et al., 2018; Pan et al., 2015; Skakun et al., 2017; Zheng et al., 2015) due to its sensitivity to chlorophyll and hence its correlation with crop phenological changes. Schuster et al. (2012) studied the use of red edge NDVI and red NDVI from RapidEye images to improve overall land use classification in west Berlin, Germany for classes such as agricultural areas, water bodies, vegetation and urban surfaces. The authors found out that improvement in land use classification results when using red edge NDVI, depended on the classes being investigated. Thus, the effects of red edge NDVI are class-specific and based on the chlorophyll content within the leaves for the class. The study by Gerstmann et al. (2016) revealed that red edge NDVI could better discriminate between winter barley and winter wheat than the classical NDVI.

Comparing classical NDVI with red edge NDVI for corn yield prediction during early and late stages of growth, Sharma et al. (2015) concluded that in the early growth stage, the two indices did not have a difference in prediction. In contrast, in the late growth stages, red edge NDVI showed better corn yield prediction results than classical NDVI. The difference was due to the high sensitivity of red edge bands to low chlorophyll concentration (Gitelson and Merzlyak, 1997). Skakun et al. (2017) used MODIS NDVI time series data to map winter cropping for a large area. They concluded that the use of NDVI ensured robustness in the processing since the input data was little.
Similarly, MODIS NDVI time series was used to map three main crops (maize, soy and cotton) in Mato Grosso (Chen et al., 2018). Wardlow and Egbert, (2010) compared NDVI and Enhanced Vegetation Index (EVI) to map crops accurately using MODIS data in US central plains. They found out that the two vegetation indices had almost the same classification accuracies for irrigated and non- irrigated crops. Gao et al. (2000) found out that NDVI is more sensitive to chlorophyll and more advantageous than EVI to portray biophysical properties applicable across different canopies. The study using the RapidEye vegetation indices on crop type classification and their influence on classification accuracy concluded that red edge NDVI resulted in higher classification accuracy (Ustuner et al., 2014)

2.3. Pixel-based and object-based classification comparison

Duro et al. (2012) examined pixel-based and object-based classification ability to map land cover using decision trees, Random Forest (RF) and Support Vector Machine (SVM) and concluded that there was no statistically significant difference between pixel-based and object-based classification. They also found the segmentation process to be time consuming; hence object-based classification took more time.
The potential of both pixel and object-based classification to map crop systems using five supervised classification algorithms has been studied as well as the effect of improved spatial resolution on classification (Castillejo-González et al., 2009). The study concluded that object-based classification outperformed pixel-based classification in terms of accuracy. Additionally, improvement in spatial resolution led to an increase in classification accuracy. Robertson and King, (2011) compared the classification accuracy between pixel-based classification and object-based classification in land use/land cover mapping in Canada using Landsat Thematic Mapper. The authors concluded that the overall accuracies of the two classifiers were not significantly different using McNemar's test.
Belgiu and Csillik (2018) studied the performance of TWDTW in cropland mapping using S2 images for both pixel and object-based classification in three study areas. In their conclusion, they noted that object-based classification outperformed pixel-based classification in terms of quality of the output products as well as the computational time. Additionally, when comparing RF with TWDTW, the authors found that RF produced better classification results than TWDTW in the region with high within-field heterogeneity.
The study by Valero et al. (2016) focused on comparing pixel and object-based classification to determine binary cropland mask using the framework of Sen2Agri using 12 test sites using SPOT4, RapidEye and Landsat8 as a proxy to S2. The authors concluded that the two methods yielded similar results. Yet, object-based classification resulted in less noisy classification maps.

2.4. Dynamic time warping (DTW) for crop mapping

DTW has been used in agriculture mapping in different forms. Maus et al. (2016) studied DTW for land cover and land use classification using remote time series and the importance of time temporal constraint. In their study, they concluded that although DTW works well for shape matching; TWDTW improves on DTW by generating a better classification accuracy for land use and land cover classification using remote sensing time series. Petitjean et al. (2012) introduced DTW to deal with irregular time series for land use and land cover mapping. The authors concluded that DTW was able to solve the main challenges arising from high temporal resolution satellite image series such as irregular sampling in temporal dimension and

comparison of pairs of time series having different number of samples. Belgiu and Csillik, (2018) studied the performance of TWDTW method to map cropland in different agroecosystems. The authors compared the results of TWDTW method using pixel-based and object-based analysis with the results from RF; TWDTW was proved to be less sensitive to training samples. The tcDTW has been used for crop mapping, whereby the classification using tcDTW was compared with DTW without constraints (Csillik et al., 2019). The authors concluded that tcDTW resulted in higher overall classification accuracy than DTW. Manabe et al. (2018) adopted the use of TWDTW and EVI from MODIS to develop a framework for integrated crop and livestock (ICL). They found out that the framework was able to map ICL areas within Sinop, Mato Grosso region. However, there were misclassifications between pasture and crops. Li and Bijker, (2019) used TWDTW dissimilarity measure with SPRING search strategy (twDTWS) to study the use of both scatter coefficients and features decomposed from Sentinel-1A(S1A) dual-polarization to map vegetables. The authors discovered that using twDTWS, it was possible to classify vegetable from S1A, decomposed features from S1A did not affect overall accuracy, and twDTWS had low sensitivity to relative weights between time factor and feature similarity.

Guan et al. (2016) used DTW-distance-based similarity to map rice growing in Vietnam. They found that the results generated had a high correlation with the statistical data as proof that the results produced were reliable.

Dong et al. (2020) used phenology TWDTW to map winter wheat in a large area of North China based on NDPI (calculated by replacing red band in equation(1) with red-SWIR bands to minimise sensitivity to soil background; snowmelt effect (Wang et al., 2017)). The classification achieved an overall accuracy of 89.98% with the planting area generated from the classification agreeing with the municipal census data.

Due to its ability to calculate optimal alignment between two-time series, DTW was adopted to map rice in Japan (Chen et al., 2015). The authors were able to map rice and damages caused by the Tsunami on the crop. The resulting information from the classification showed a high correlation of 0.77 with the area's statistics.

Guan et al. (2018) made use of open-boundary locally weighted dynamic time warping (OLWDTW) to classify rice paddy and dryland crops. The authors observed that OLWDTW resulted in higher classification accuracy than usual DTW. Although the OLWDTW had a higher overall accuracy, it produced low accuracy for dryland crops due to the small plots of dryland crops.

DTW was applied to map single cropping, double cropping and horticulture in India using MODIS NDVI (Mondal and Jeganathan, 2018). The authors compared the use of Euclidean distance (ED) with DTW results; DTW gave better overall classification accuracy than ED. The authors found out that DTW gave better results in classifying single and double cropping than for horticulture.

2.5. Use of PS and S2 images in agricultural mapping

Mudereri et al. (2019) evaluated the strength of S2 and PS images to map Striga weed within maize plantation. They concluded that S2 and PS images produced high classification accuracies in detecting Striga weeds though PS images showed slightly higher classification accuracy. PS images were used to establish a sample size sufficient to estimate humus content in the soil for precision agriculture in Japan (Odagawa et al., 2019). The authors were able to produce high accuracy models to estimate humus content using PS images. Houborg and McCabe (2016) evaluated the suitability of PS images for mapping alfalfa, corn, carrots and other vegetables in the irrigated area in Riyadh; Saudi Arabia. They found out that the high spatial resolution increases the ability to discriminate within-field variability in the growth period of crops.

The efficiency of S2, PS images, Geo-Eye-1, WorldView-2 and WorldView-3 on estimating sorghum yield was recently assessed (Lobell et al., 2020). The authors concluded that the satellite sensors exhibited similarity in their performance (Lobell et al., 2020). Liu et al. (2019) used PS images to develop a model to

map forage production in California. The study demonstrated the utility of satellite images to generate spatially explicit and near real-time forage estimates as the generated models agreed well with field measurements with R^2 of 0.8. Breunig et al. (2020) used PS images to delineate agricultural management zones in Brazil based on the assumption that above-ground biomass of cover crops (white oats, forage turnip and rye) are correlated to cash crop (maize and soybean) yields. The authors conclude that the generated management zones maps can guide farmers before cash crop farming. Their analysis also concluded that there was a high correlation between cover crops and cash crops with correlation coefficient (r) values of more than 0.7 for all cover crops.

2.6. Smallholder farm mapping

Different approaches which range from machine learning to deep learning, have been adopted to map smallholder farms using remotely sensed images. Persello et al. (2019) mapped smallholder farms using Worldview-2/3 imagery to delineate agricultural fields using fully convolutional networks. They were able to segment the study areas into different agricultural fields, obtaining an F-score of 0.7 and 0.6 for the two study sites. Lambert et al. (2018) estimated smallholder farms crop production at the village level using S2 images in Mali cotton belt. They learned that S2 provided an opportunity to map smallholder crop types with high classification overall accuracy, i.e. 80%. To overcome the challenge of smaller smallholder farms (i.e. smaller than the resolution of the freely available images)Neigh et al. (2018) used Worldview-1/2 imagery to map smallholder crop area in the Tigray area of Ethiopia. The authors were able to estimate 37% of cropped area in the study area. In mapping smallholder farming, Jin et al. (2017) evaluated crop yield estimates using Skysat, RapidEye and S2 images in western Kenya. This study revealed that the generated model was able to capture within and between field heterogeneity. In an attempt to measure smallholder yields at national and global scales, Jin et al. (2019) generated countrywide 10m resolution maize yields maps for Kenya and Tanzania using S1 and S2 imagery. Aguilar et al. (2018) adopted the use of a cloud-based ensemble classifier to map smallholder systems in West Africa using Worldview-2 data. Their experiments proved that ensemble classifiers (Maximum Entropy model (MaxEnt), SVM with the linear kernel (SVML), SVM with the polynomial kernel (SVMP) and SVM with Gaussian kernel (SVMR)) could be adopted to map smallholder farms in West Africa, where the classier attained an overall accuracy of 75.9%. Jain et al. (2017) worked on an automated method to map winter cropped area in smallholder farms in India. The authors used MODIS data. They found out that although the automated method was able to map winter cropped area for the country, the overall accuracy of the classification varied largely as per the level of heterogeneity within the smallholder farms. Xie et al. (2019) made use of deep convolutional neural networks(CNN) to map smallholder farms in four areas in China using GaoFen-1 images. This study showed that CNN produced better classification accuracy than RF classifier.

3. STUDY AREA AND MATERIALS

This part of the report gives details on the study area and materials used in the study.

3.1. Study Area

The study area is located in Diepenheim, the Netherlands. It is located in Hof van Twente municipality in Overijssel province, as shown in

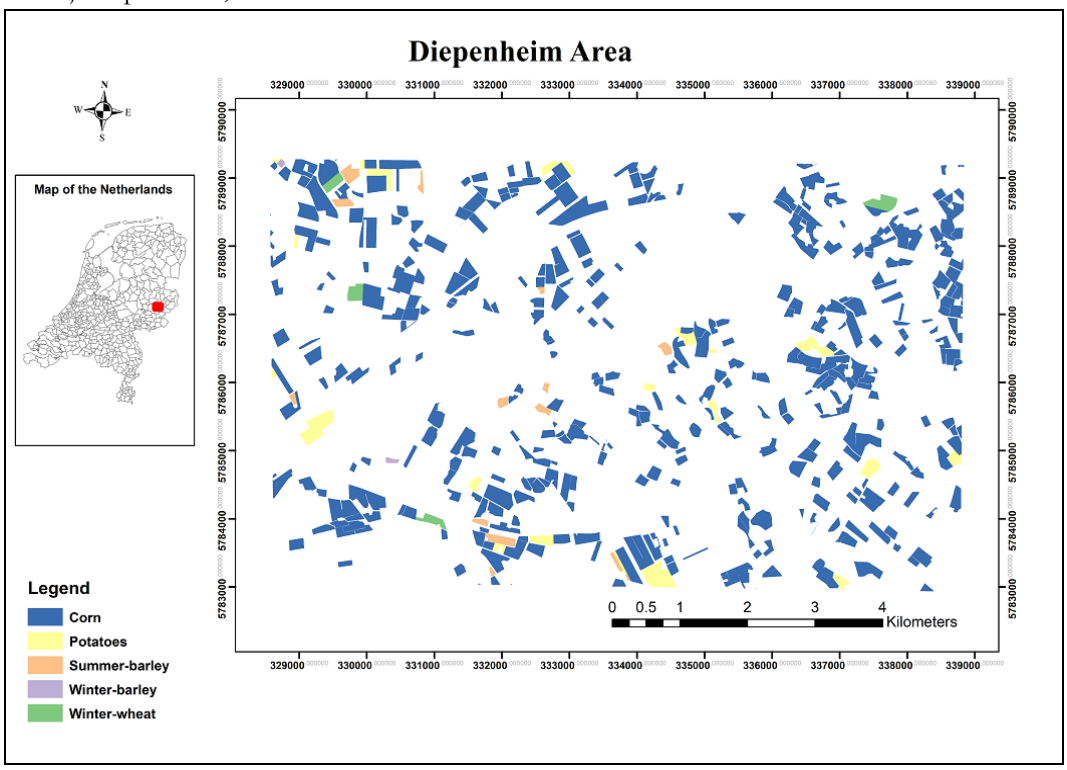

Figure 1. Diepenheim is one of the areas in the country with smallholder farms. According to the data obtained from National geo register, both winter and summer crops are cultivated (Kadaster, n.d.). The main crops grown in the area include corn, summer and winter barley, winter wheat and potatoes. Corn is usually planted in April/May and harvested in September; potatoes are as well planted in April and May for half-late and late potatoes and harvested in September and October respectively. Winter barley and winter wheat are sown in October and mid-February respectively and harvested in August. Summer barley is planted in around February/March and harvested in August. The crop calendar shows the planting and harvesting time of the crops (Figure 2). The study area is approximately 63.66 km^2.

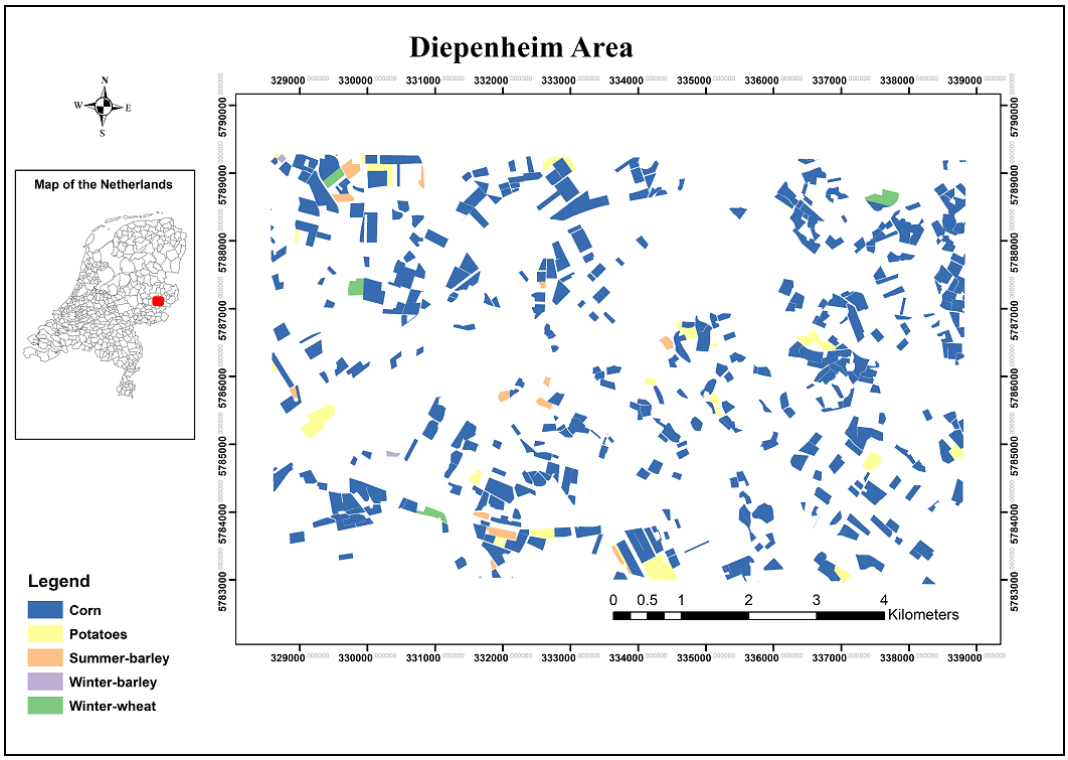

Figure 1: Diepenheim study Area showing crops grown in the year 2018

crop	Month	Jan				Feb				Mar				Apr				May				Jun				Jul				Aug				Sep				Oct				Nov				Dec			
	Weeks	I	II	II	IV	I	II	II	IV	I	II	II	IV	I	II	II	IV	I	II	II	IV	I	II	II	IV	I	II	II	IV	I	II	II	IV	I	II	II	IV	I	II	II	IV	I	II	II	IV	I	II	II	IV
Corn																																																	
Potatoes																																																	
Summer barley																																																
Winter barley																																																
Winter wheat																																																
	Key		Early-season												Mid-season												Late-season																					

Figure 2: Crop calendar for crops grown in Diepenheim

Source: Brink et al., 2008; Darwinkel, 1997; "Gerst - Wikipedia," n.d., "Potato - Wikipedia," n.d.

3.2. Material

3.2.1. Satellite data

PS satellite images were downloaded from PlanetScope labs portal (https://www.planet.com/products/planet-imagery/). Area of interest (AOI) was created using Google Earth.

The AOI was converted to Keyhole Markup Language (KML) file format and uploaded in the portal to mark the download area. Then, filters for cloud cover and coverage was defined at 0% and 100% respectively. The available PS Analytic Ortho Scene product 4 spectral bands (blue, green, red, near-infrared) images were downloaded, as shown in Table 1. PS analytic ortho scene was selected for the study. The images were already radiometrically and geometrically corrected (Planet, 2019). The PS images downloaded were captured in scenes with small tiles for the same date. Complete image for each date, as shown in Table 1 was realised by mosaicking two PS image tiles for that specific date. This process was repeated for all images downloaded for all months. Due to the availability of winter crops within the study area, more images were sought for January, November and December. January image had a cloud cover of

40%, whereas the November image had a cloud cover of 1%. December images had a cloud cover of over 45%. From the metadata of the PS image tiles fitting (selected) the study area had 0.36% cloud cover, 0.01% cloud cover for November image and over 45% for the December images. Hence, the December image could not provide useful information for the current study.

Cloud free images were downloaded for February, March, April, May, June, July, August September and October for the year 2018. The summary in Table 1 shows the used images.

Other images were downloaded for evaluation of the suitability of temporal capability of the PS images. The filter for cloud cover was set at 5% and area coverage at 100%. More dense images were needed to evaluate the temporal suitability of PS images to map crops in smallholder farm systems; hence additional PS images downloaded are as shown in Table 2.

Table 1: Time series data (PS images) showing cloud cover (C.C), Date of the year (DoY), months and specific dates for the images used in Diepenheim study area

PlanetScope Images for Area around Diepenheim			
Months	**date**	**C.C %**	**DoY**
January	21-Jan	0.36	21
February	16-Feb	0	47
March	20-Mar	0	79
April	18-Apr	0	108
May	08-May	0	128
June	30-Jun	0	181
July	01-Jul	0	182
August	02-Aug	0	214
September	25-Sep	0	268
October	28-Oct	0	303
November	15-Nov	0.01	319

Table 2: Additional PS images to assess the suitability of the temporal nature of PS Images to map crops in smallholder farm systems

Extra PlanetScope Images for Area around Diepenheim			
Months	**date**	**C.C %**	**DoY**
March	2-Mar	0.08	61
March	31-Mar	0.04	90
May	28-May	0.01	148
June	6-Jun	0.01	157
July	16-Jul	0.00	197
August	07-Aug	0.02	217
September	05-Sep	0.05	248
October	12-Oct	0.05	285

S2 images were downloaded to evaluate the suitability of PS bands for crop mapping in smallholder farms. Ten images acquired by multispectral instrument (MSI) sensor onboard S2 platform (Table 3) were downloaded from the Copernicus Open Access Hub (https://scihub.copernicus.eu/).

Table 3: S2 images to spectrally evaluate the suitability of PS images for crop mapping in smallholder farms

S2 Images for Area around Diepenheim			
Months	**Date**	**C.C %**	**DoY**
January	08-Jan	41.89	8
February	07-Feb	1.29	38
March	19-Mar	1.5	78
April	18-Apr	43.23	108
May	08-May	0.79	128
June	07-Jun	6.74	158
July	27-Jul	7.67	208
August	06-Aug	0.69	218
September	30-Sep	4.9	273
October	10-Oct	0.4	283

3.2.2. Reference data

The reference data were downloaded from the Dutch National geo-register. The Dutch National geo-register is the source of geoinformation in the Netherlands where 6833 datasets, services and maps are stored. The Dutch National geo-register contains data in different categories such as geoscientific data, agriculture and livestock height, amongst others. Basic registration crop plot (BRP) data was downloaded (https://bit.ly/2URJ2HU) for the year 2018. The files were provided in ESRI format file database under the terms of use for open data that allows data to be used by both private individuals and companies in their own applications (http://www.rijksoverheid.nl/opendata/voorwaarden). The data contained both agricultural plots and cultivated crops. The boundaries of the agricultural plots are based on Dutch agricultural area, while cultivated crops are shared by the farmers (Kadaster, n.d.).

3.2.3. Software used in the study

The main softwares used in this work are depicted in Table 4.

Table 4: Software used in the data processing

Software	Type	Analysis
ArcGIS 10.7.1	Commercial	Co-registration Crop mask preparation
eCognition	Commercial	Object-based classification
ERDAS imagine 2018	Commercial	Mosaicking PS images Visual interpretation of pixel alignment Visual interpretation of segmentation
ENVI 5.5	Commercial	Segmentation evaluation
QGIS3.10.0	Open-source	Image pixel alignment Resampling of S2 images
R	Open-source	Programming

Codes adopted in the study: Maus et al. (2016); Marpu et al. (2010); Csillik et al. (2019) and codes used in GFM course practicals.

4. METHODOLOGY

4.1. Pre-processing

This part of the report gives details on the pre-processing done on the data sets acquired for the study.

4.1.1. Crop data set and PS data co-registration

The crop dataset was projected in "Rijksdriehoekscoördinaten" (RD) New coordinates (Dutch national coordinate system) (EPSG, 2005) and Amersfoort datum. PS images were projected in Universal Traverse Mercator (UTM) zone 32 North (N) coordinates and WG84 datum. Thus, a misalignment of the two datasets arose. Therefore, crop dataset was projected to geographic coordinate WGS1984 datum and then re-projected to UTM zone 32N. After this process, the two datasets were co-registered. The AOI was realised by visually observing small irregular-shaped fields which have not been put under land consolidation. Land consolidation refers to changes in the property resulting from the performance of works or arrangement of land use in order to meet particular objectives (Brink, 2004). Land consolidation is a planned process of aggregating smallholder farms to aid agricultural mechanisation for high agricultural production. Additionally, land consolidation is a statutory tool used to resolve Netherlands land-use resolutions at both national and provincial levels (Brink, 2004). The tool allows for land acquisition, land exchange and land development.

Before calculation of NDVI values, all images were co-registered. This was done using ERDAS Imagine software, where one of the images was used as a reference image. The rest of the images were checked for alignment of pixels against it.

4.2. Sampling strategy

An internal buffer of 10 meters was generated within each polygon (crop field) to avoid border effect. Due to border effect, crops at the centre of a plot have different growth pattern from the one at the borders. The border effect might result in growth difference either due to a mixture of different crops or less or no fertiliser reaching the boundaries. After extracting the buffer zone from each polygon, points were randomly generated within.

The random points generated were then joined with their respective polygons. Stratified random sampling was used since it allows for the creation of strata for each crop (Foody, 2009). These strata allowed every crop to be selected in the sample data. A 50 pixels sample was extracted for each crop polygon. For the training data sample, the first crop polygons for each crop were selected. The polygons used to generate training data were excluded for the sampling done for validation data. This was done to separate the training data from the validation data clearly. The validation data was generated from the remaining polygons, where 50 samples were sampled for each class (Congalton, 2001).

Initially, corn had three classes that are corncob mix, corn cutting and corn grain. Similarly, potatoes had three different classes; starch potatoes, seed potatoes and consumption potatoes. The three classes for corn and potatoes were merged to form corn and potatoes class respectively. This is the reason why these two crops have more than 50 samples. The merge was motivated by the fact that the crops had almost the same resemblance in their temporal profiles. The distribution of training and validation data is shown in Table 5. The spatial distribution of the training and validation data is depicted in Figure 3.

Table 5: Training and validation data

Label	Training samples (pixels)	Validation samples (pixels)
Corn	150	150
Potatoes	150	150
Summer barley	50	50
Winter barley	50	31
Winter wheat	50	50
Total	450	450

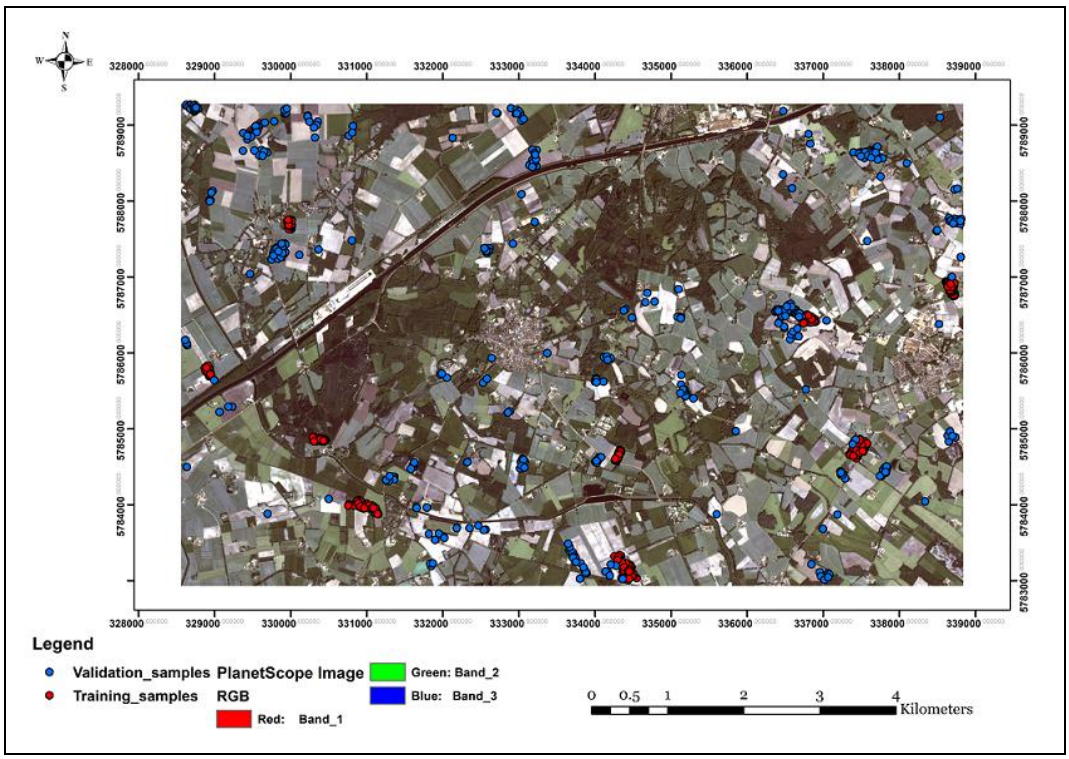

Figure 3: PlanetScope image and spatial distribution of training and validation samples

4.3. NDVI time series

NDVI has been proven to be a reliable vegetation index for crop mapping using satellite image time series (Belgiu and Csillik, 2018). Due to its sensitivity to chlorophyll, NDVI can explain the crop phenology at different development stages. For example, if there is no crop present on the field the NDVI values will be near zero or negative, as soon as the crop starts growing the NDVI values increase gradually until they reach a value close to one when the crop is fully grown, and then they start decreasing at the crop senescence. Therefore, NDVI is successfully used to discriminate different crops. In addition, NDVI reduces the dimensionality of the data, hence reducing the computational cost for the classifier. NDVI was calculated for the 11 PS images acquired, using the NDVI formula (Rouse et al., 1973) provided in equation(1):

$$NDVI = \frac{NIR - red}{NIR + red} \qquad \text{equation(1)}$$

Where; NIR is the reflectance in the near-infrared band(NIR)
red is the reflectance in the red band

Then, NDVI was calculated for the 11 PS images and resulting NDVI layers were stacked together to form a PS NDVI time series stack which was used for classification of the crops.

4.4. Crop mask

The crop mask is a binary map containing cropped areas and non-cropped areas. The crop data extracted from geo-register was used to make a crop mask for the study area. A shapefile containing all crops was generated. The crop mask was used to eliminate non-crop areas within the PS NDVI time series stack. The masked PS NDVI time series stack was then supplied to the classifiers for classification.

4.5. Segmentation

This study adopts the use of mean-shift segmentation algorithm (Wu and Yang, 2007). Mean shift is a non-parametric algorithm for segmentation. The mean-shift procedure runs iterations initialized at each data point to have each mode define a segment, with all points that converge at that point belonging to the same segment (Hennig et al., 2015). The algorithm does not require prior specification of the clusters, but they are automatically determined. Mean shift segmentation has been proved to be successful in image segmentation in agriculture (Jantakat et al., 2019; Ozdarici-Ok and Akyurek, 2014; Su et al., 2015; Xu et al., 2019).

The parameters used for this segmentation are kernel bandwidth (h), Nearest neighbours(nN) and the number of iterations. The kernel bandwidth defines the size of the window. Increasing values of h ensure that two segments located closer than initial h are merged to form one segment. Therefore, large values of h lead to larger segments. nN is useful in speeding up the approximation of the kernel density estimate. Thus, large values of nN lead to longer computations. Iterations are defined to give the lower bound of the mean shift vector to stop the iterations since the mean shift has infinite convergence when using a uniform kernel (Comaniciu and Meer, 2002).

These segmentation parameters were manually tuned. First segmentation was done with single date PS images as input data. The parameters were tuned manually using different values. That is h =200, 100, 50, 2, 1, 0.5 ,0.05 nN = 7 10, 15, and 100, 300, 400 , 700 , 1000 iterations. Through visual interpretation of the output segments against the original images, parameters h = 0.05, nN =15 and 1000 iterations were chosen as the best results. In the next step, segmentation was performed on a stack of all 11 available PS images. Same parameters were tuned using the values tested in the previous segmentation. By visual interpretation, the best result was obtained with the following parameters: h= 0.05, nN=15 and 1000 iteration. Segmentation using 11 images was found to provide a better fit to the field boundaries than the previous segmentation obtained using single PS image. Thus, the segmentation using the 11 images was used for object-based classification.

4.6. TWDTW

This study makes use of TWDTW classifier. DTW method (Sakoe and Chiba, 1978) accounts for the non-linear shifts in vegetation index curves caused by a variety of factors such as different weather conditions and different agricultural practices. It has previously been successfully used for agricultural mapping (Petitjean et al. 2012; Belgiu and Csillik, 2018; Li and Bijker, 2019) and to assess similarities between different climatic zones (Netzel and Stepinski, 2018). The classifier has also been used in the study done by Maus et al., (2016) for land use and land cover mapping. TWDTW searches all the patterns on time series and similar matches periods that are associated with the respective class (Simoes et al., 2017). Logistic TWDTW classifier is used in this study since it provides better accuracy than the linear logistic.

4.6.1. DTW

DTW matches a sequence of time series associated with each pixel location to the sample of the expected class. Below is an illustration of how DTW algorithm is applied for each pixel: Consider two time series matrices **P** and **Q**. Let the length of **P** be t; such that **P**= $\{p_1,p_2,\ldots\ldots\ldots P_t\}$ and the length of **Q** be s; such that **Q** = $\{q_1,q_2,\ldots\ldots\ldots q_s\}$. The DTW algorithm will begin by constructing a matrix (M) t x s; that is $\mathbf{M}_{t\,x\,s}$. From the computed matrix **M**, whose absolute elements are the difference between p and q defined as p ∈ **P** ∀ i = 1, ..., t and q ∈ **Q** ∀ i = 1, ..., s the DTW algorithm will compute an accumulated cost matrix **N** by the recursive sum of the minimal distances such that :

$$n_{ij} = M_{ij} + min\{m_{i-1,j} m_{i-1,j-1} m_{i,j-1}\} \qquad \text{equation(2)}$$

$$n_{ij} = \begin{cases} M_{ij} & i = 1, j = 1 \\ \sum_{k}^{i} M_{kj} & 1 < i \leq t, j = 1 \\ \sum_{k}^{j} M_{i,k} & i = 1, 1 < j \leq s \end{cases} \qquad \text{equation(3)}$$

The DTW algorithm runs iteration within the **N** to finds the matches between **P** and **Q** using the shortest cost distance between the two time series. Time-weighted extension of DTW introduced by Maus et al. (2019) adds a temporal cost to matrix **M.** Temporal cost can be computed in using both linear and logistic model. In this study, the logistic model with parameters alpha and beta is preferred as gives better accuracy than the linear model (Maus et al., 2016). DTW matches each pattern to input time series independently from the others; thus, the patterns with lowest DTW distance are used to generate a landcover map (Maus et al., 2016).

4.6.2. Pixel-based classification

The *dtwSat* implemented by Maus et al. (2019) in R was used in the processing. From the PS NDVI time series stack and the timeline vector (with image acquisition dates), a PS raster time series was generated. A time series of the reference data (Table 5) was extracted from PS raster time series.

The extracted training time series was used for generation of the temporal patterns and to classify the PS raster time series. Using a temporal frequency of 2 for smoothed cycles and a Generalized Additive Model (GAM) (Wood, 2011) smoothing formula (y ~ s(x, k=7)) the temporal patterns shown in Figure 4 was created. Several parameters were tried for logistic weight function, for alpha =-0.1, 0.1 and beta = 80, 90, 100 and 120. The best accuracy results were realised when the parameters were set as for alpha = -0.1 and beta =90. Thus, alpha= -0.1 and beta = 90 is adopted for the pixel-based classification.

Using TWDTW analyses, each pixel location in the PS raster times series was assigned into a class using temporal profiles generated from the training data. Subsequently, the output generated was used to classify the raster into different crop types from the shortest cost distance (unique value).

Explanation on the following parts of the classifier; codes source: Maus et al., (2019)

(i)

```
\temporal_patterns <- createPatterns(training_ts, freq = 2,
formula = y ~ s(x, k=7))
```

The function createpatterns is used to produce temporal patterns based on training samples (Maus et al., 2016).

where; training_ts is a time series object.

freq is the sampling frequency of the output patterns
y ~ s(x, *k*=7)
is a general additive model which is the sum of a smooth function of the variables
where; *k* is the basis of dimension
x is the design matrix, Wood, (2017)

The models use splines to reduce approximation error. A spline is a curve formed by cubic polynomials joined together by knots. *k* sets the maximum number of degrees of freedom allowed for the model. From createPatterns method, temporal profiles were extracted from PS NDVI time series raster for the five main crops (corn, potatoes, summer barley, winter barley and winter wheat), as shown in Figure 4

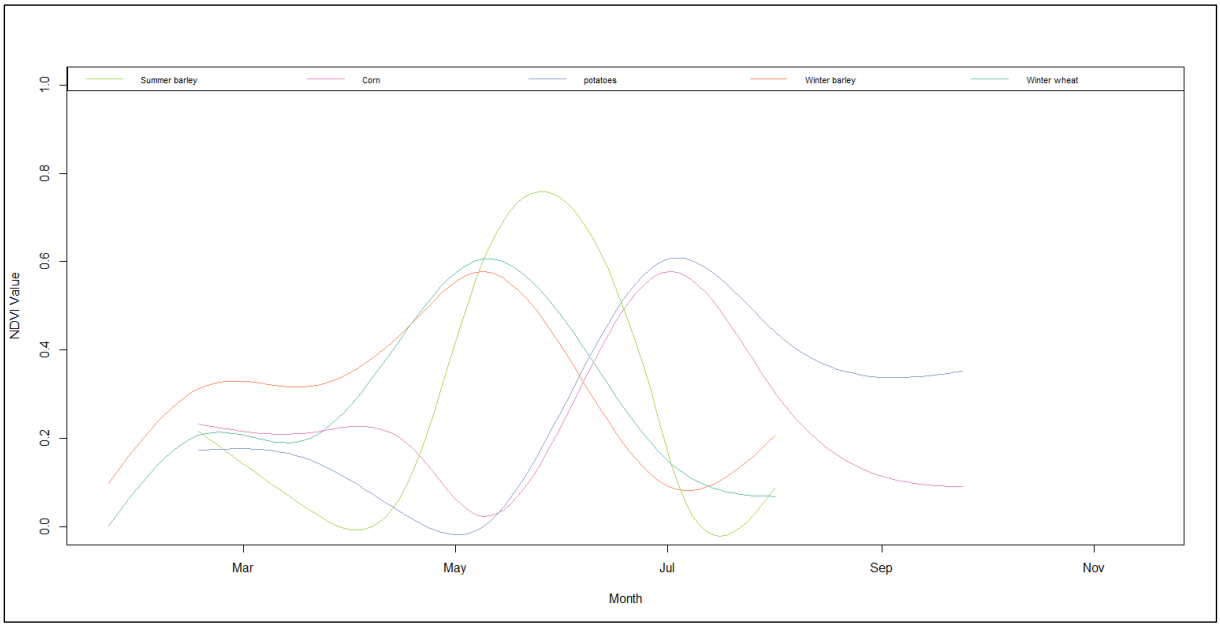

Figure 4: Temporal profiles of NDVI summer barley, corn, potatoes, winter barley and winter wheat generated using the training data

(ii)

```
\log_fun <- logisticWeight(alpha = -0.1, beta = 90)
```

Logistic weight function builds a time-weighted logistic function to compute the TWDTW local matrix

Where; beta is the time constraint
alpha is the steepness of the logistic weight

The logisticWeight adds a time constraint (time-weight) to DTW analysis. In this case, beta gives the time constraint in days. For example, if beta = 90, it means that a constraint of 90 days was defined. The constraint allows the classifier to provide less weight for time warps less than 90 days and higher cost for more than 90 days hence, better performance of the TWDTW classifier(Maus et al., 2016).

4.6.3. Object-based classification

The object-based classification was done using a tcDTW algorithm implemented in eCognition Developer software (Csillik et al., 2019). The difference between TWDTW and tcDTW is that TWDTW a linear or logistic weight to the model while for tcDTW all elements within a time delay are considered in computation(Csillik et al., 2019; Maus et al., 2015). The tcDTW algorithm is intended to limit the computational cost of the DTW matrix to a predefined time delay. An element of the matrix is computed only when the date difference between the two dates of the compared sequences is small or equal to a set

time delay (Csillik et al., 2019). The tcDTW works on a stack of layers, objects of a segmented image and the training data whereby, the objects are classified to classes into which, each object has minimum dissimilarity value (Csillik et al., 2019).
Using tcDTW single band classification, the time delay was put at 50, 65, 70, 80 and 90 days. These values were used in consideration of temporal profiles generated for all crops in the study. The best accuracy was attained at a time delay of 65 and 70 days. Therefore, the 65 days was used for this classification.

4.7. Accuracy Assessment

The accuracy of both pixel-based and object-based classification is performed using the 450 validation samples presented in Table 1. The confusion matrix generated will help generate the producers and users accuracy as well as overall accuracy (Congalton, 1991). Evaluation of classification results for pixel-based and object-based classification was done using McNemar's test (McNemar, 1947). McNemar's test is a nonparametric statistical test for paired data. The test assumes a Chi-square ($\chi 2$) test for comparing the classification results and applied on a 2x2 contingency table. For instance, using model 1 and model 2 and their correct and incorrect class allocation, as shown in Table 6.

Table 6: Comparison of classification results between model 1 and model 2

		Model_2	
		correct	incorrect
Model_1	correct	**a**	**b**
	Incorrect	**c**	**d**

McNemar's Chi-square test can be computed as shown in equation (4) (Foody and Mathur, 2004):

$$x^2 = \frac{(b-c)^2}{b+c} \qquad \text{equation(4)}$$

If the calculated $\chi 2$ is less than 0.05 p-value at 95% confidence, it can be concluded that the output of the two classification methods are statistically significantly different. Else, if the calculated $\chi 2$ is greater than 0.05, the two classifications are not statistically significantly different.

4.8. Assessment of the suitability of PS images for mapping smallholder farm systems

Spatial, temporal and spectral suitability of PS images to map crops in smallholder farm systems were studied. The section entails the quantitative evaluation of the segmentation as well as of the temporal and spectral resolutions of PS images.

4.8.1. Spatial resolution

Segmentation goodness was analysed in order to evaluate the suitability of spatial resolution of PS images to map crops. Segmentation goodness is defined as how well the segmentation splits sets of the objects of interest (Clinton et al., 2010). The goodness of segmentation was assessed based on the level of under-segmentation and over-segmentation. According to Marpu et al. (2010), over-segmentation occurs when the objects of interest are segmented into smaller sub-objects, whereas under-segmentation occurs if segmentation results in parts of an object become part of another object. The segmentation evaluation is based on the definition of over-segmentation and under segmentation. The evaluation makes consideration of sub-objects that overlap with 55% pixels from the reference object as useful. Figure 5 illustrates the concept of lost and gained pixels in the segmentation.
Extra pixels, as shown in Figure 5, are the ones that are part of the sub-object that has an adequate number of pixels from the reference object but are not part of that reference object (Marpu et al., 2010).

Lost pixels are those pixels that are part of the reference object, but are also part of the sub-objects that do not contain the sufficient number of pixels (55%) from the reference object.
Over-segmentation was evaluated based on the percentage of the biggest area after excluding extra and lost pixels. In contrast, under-segmentation was assessed based on lost pixels, extra pixels and the number of reference objects that lost or gained more than 25% of their area. (Marpu et al., 2010).
The segmentation evaluation was based on criteria highlights below:

- Percentage of the area of the biggest sub-object
- Percentage area of the lost pixels
- Percentage area of the extra pixels
- The number of reference objects that lost more than 25% of the pixels
- The number of objects which gained more than 25% of the pixels

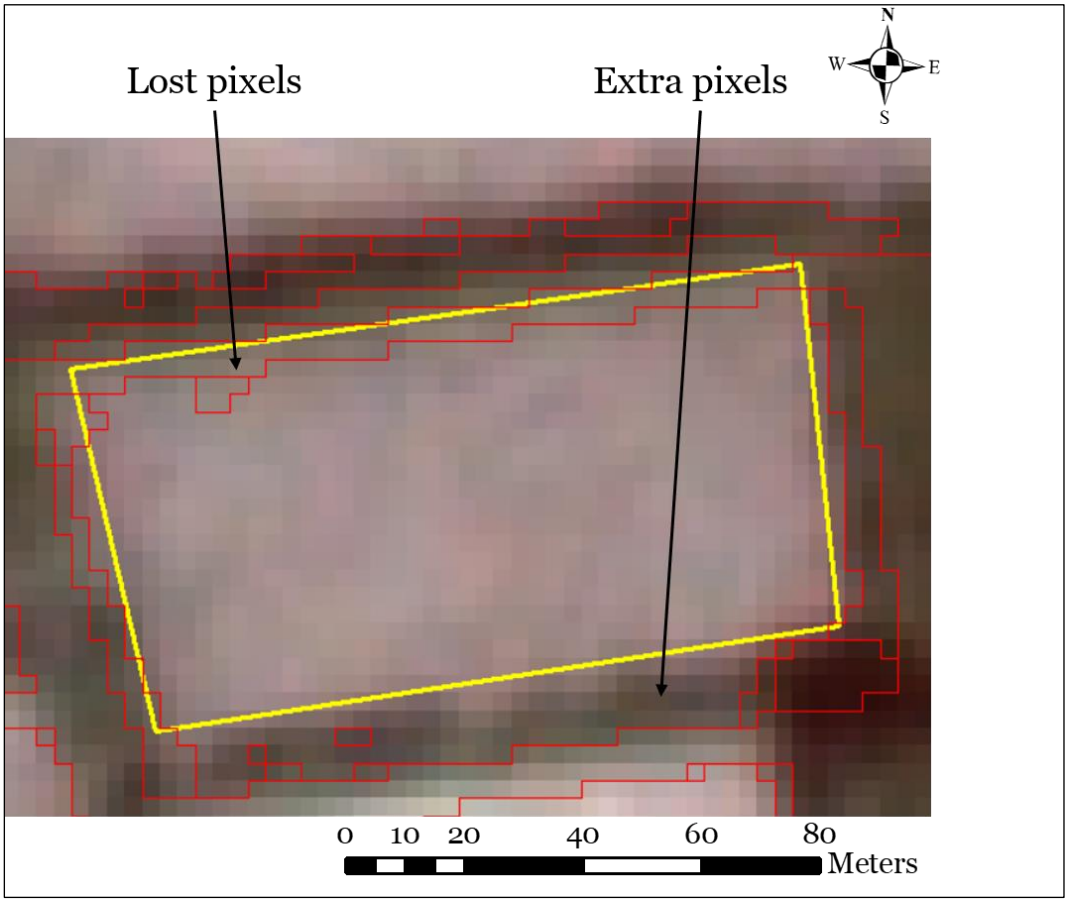

Figure 5: An illustration of extra and lost pixels. The yellow box shows a reference object (polygon) overlaid with the segmentation

The reference objects for over-segmentation and under-segmentation evaluation were the polygons used to generate the crop mask.

4.8.2. Temporal resolution

To evaluate temporal resolution, 18 images instead of 11 images as previously used in classification were considered for testing the advantages of having a larger number of images as input. NDVI was calculated for the additional images and stacked together with the initial NDVI forming a time series of 18 NDVI layers. The crop areas were masked from the NDVI time series. The resulting NDVI was used to classify crop types within the study area using the pixel-based method of classification. The parameters adopted for the classification were alpha = -0.1 and beta = 90.

4.8.3. Spectral resolution

PS images have four spectral bands: red, blue, green and NIR. For evaluation of the suitability of the spectral resolution of PS images to map crops in smallholder farm systems, S2 images are used. The evaluation made use of the red band, NIR and red edge bands. The red edge bands are believed to be sensitive to chlorophyll, which varies highly across different crops (Xie et al., 2018). In order to evaluate the suitability of the spectral resolution of PS images to map crops, this study compares the classification accuracy generated using classical NDVI with those obtained using red edge NDVI. Red edge NDVI was calculated using three different equations; equation(5) (Fernández-Manso et al., 2016), equation(6) (Gitelson and Merzlyak, 1994) and equation(7) (own). S2 images were downloaded, as shown in Table 3. For calculation of classical NDVI, only band4 (red) and band8 (NIR) were used. Since band4 and band8 have a 10-metre resolution (t.ly/pZGKn), they were resampled to 20-metre spatial resolution (resolution of red-edge bands) using the nearest neighbour resampling method.

The red-edge bands were used to calculate NDVI using both NIR (band 8) and narrow NIR (band 8A) (Fernández-Manso et al., 2016). The formula for calculation of red edge NDVI (NDVIren) using narrow NIR as suggested by Fernández-Manso et al. (2016) is shown below:

$$NDVIren = \frac{Band8A - i}{Band8A + i}; \quad where\ i = \text{band5}, \text{band6}, \text{band7} \qquad \text{equation(5)}$$

The calculation for red edge NDVI using NIR (NDVIre) was performed as per the formula proposed by Gitelson and Merzlyak (1994):

$$NDVIre = \frac{Band8 - i}{Band8 + i}; \quad where\ i = \text{band5}, \text{band6}, \text{band7} \qquad \text{equation(6)}$$

The pixel alignment for the S2 images was inspected. It was found that for January, February, March, April, June and October images, the pixels were aligned. However, for May, July, August and September, images pixels had a minor shift when visually inspected against the other image pixels. Using June image as a reference image, these images were aligned using QGIS raster alignment tool. Then, the classical NDVI was calculated for the ten images using the formula in equation(1). Further $NDVI_{REA}$ was calculated by replacing the NIR band in equation(1) with rede edge and narrow NIR bands, as shown in equation (7).

$$NDVIREA = \frac{i - \text{red}}{i + \text{red}}; \quad where\ i = \text{band5}, \text{band6}, \text{band7}, \text{band8A} \qquad \text{equation(7)}$$

All NDVI time series generated from S2 images were supplied to the TWDTW classifier under the same parameters (alpha = -0.1, beta = 90). The results of the classifications were used for comparison between the output of classical NDVI and NDVIre*n*, classical NDVI and NDVIre and classical NDVI and $NDVI_{REA}$ for crop mapping. Table 7 shows the equations used to calculate all red edge NDVI.

Table 7: Summary of equations used to compute spectral indices for red-edge bands

General initial	Band specific Initial	Equation
NDVIren	NDVIren1	$NDVIren1 = \frac{\text{Band8A} - \text{Band5}}{\text{Band8A} + \text{Band5}}$
	NDVIren2	$NDVIren2 = \frac{\text{Band8A} - \text{Band6}}{\text{Band8A} + \text{Band6}}$
	NDVIren3	$NDVIren3 = \frac{Ban\,d8A - Band7}{Band8A + Band7}$
NDVIre	NDVIre1	$NDVIre1 = \frac{\text{Ban d8} - \text{Band5}}{\text{Band8} + \text{Band5}}$
	NDVIre2	$NDVIre2 = \frac{\text{Ban d8} - \text{Band6}}{\text{Band8} + \text{band6}}$
	NDVIre3	$NDVIre3 = \frac{\text{Ban d8} - \text{Band7}}{\text{Band8} + \text{Band7}}$
$NDVI_{REA}$	$NDVI_{REA}1$	$NDVIREA1 = \frac{\text{Band5} - \text{Band4}}{\text{Band5} + \text{Band4}}$
	$NDVI_{REA}2$	$NDVIREA2 = \frac{\text{Band6} - \text{Band4}}{\text{Band6} + \text{Band4}}$
	$NDVI_{REA}3$	$NDVIREA3 = \frac{\text{Ban7} - \text{Band4}}{\text{Band7} + \text{Band4}}$
	$NDVI_{REA}4$	$\text{NDVIREA4} = \frac{\text{Band8A} - \text{Band4}}{\text{Band8A} + \text{Band4}}$

5. RESULTS AND DISCUSSION

This chapter shows the results obtained from the implementation of the described methodology in order to realise the objectives of this study and their discussions. The results entail the results of both pixel-based and object-based classifications as well as the suitability of PS images to map smallholder farm systems.

5.1. Pixel-based classification results for TWDTW

The overall accuracy for the pixel-based classification was 75.78%, as shown in Table 8. Winter wheat was best classified with UA of 80%, followed by summer barley and corn with 79.49% and 76.06% UA respectively. Winter barley recorded the lowest UA due to confusion with winter wheat. Combining winter wheat and winter barley resulted in UA of 89.58% and 1.78% increase of OA to 77.56%. Winter barley demonstrated less heterogeneity with a PA of 92%, whereas summer barley exhibited the highest heterogeneity with PA of 62%. The crop map resulting from the pixel-based classification is shown in Figure 7. Through visual inspection of the resulting crop type map and the crop type map generated from data obtained from the Dutch National georegister data (Figure 6), it was evident that most crop types were correctly mapped. However, the crop type map generated by TWDTW exhibits "salt" and "pepper" classification effect since each pixel is treated independently by the classifier (Lu and Weng, 2007). Further, due to the similarity in temporal patterns (Figure 4), it was challenging to discriminate corn from potatoes. Thus, corn was classified as potatoes and vice versa. Although summer barley showed distinct temporal pattern from winter wheat and winter barley (Figure 4), there were misclassifications amongst the three crops due to spectral similarity between wheat and barley (Gerstmann et al., 2016). This is evident from the comparison between crop type map from pixel-based classification (Figure 7) and Figure 6.

Table 8: Accuracy assessment results for Pixel-based based classification using NDVI times series generated from PS images; where UA, PA and OA stands for user accuracy, producer accuracy and overall accuracy, respectively.

	Corn	**Potatoes**	**Summer barley**	**Winter barley**	**Winter wheat**	**Total**	**UA (%)**
Corn	108	26	8	0	0	142	76.06
Potatoes	38	124	5	0	0	167	74.25
Summer barley	2	0	31	0	6	39	79.49
Winter barley	2	0	2	46	12	62	74.19
Winter wheat	0	0	4	4	32	40	80
Total	150	150	50	50	50	450	
PA (%)	72	82.70	62	92	64	**OA (%)**	**75.78**

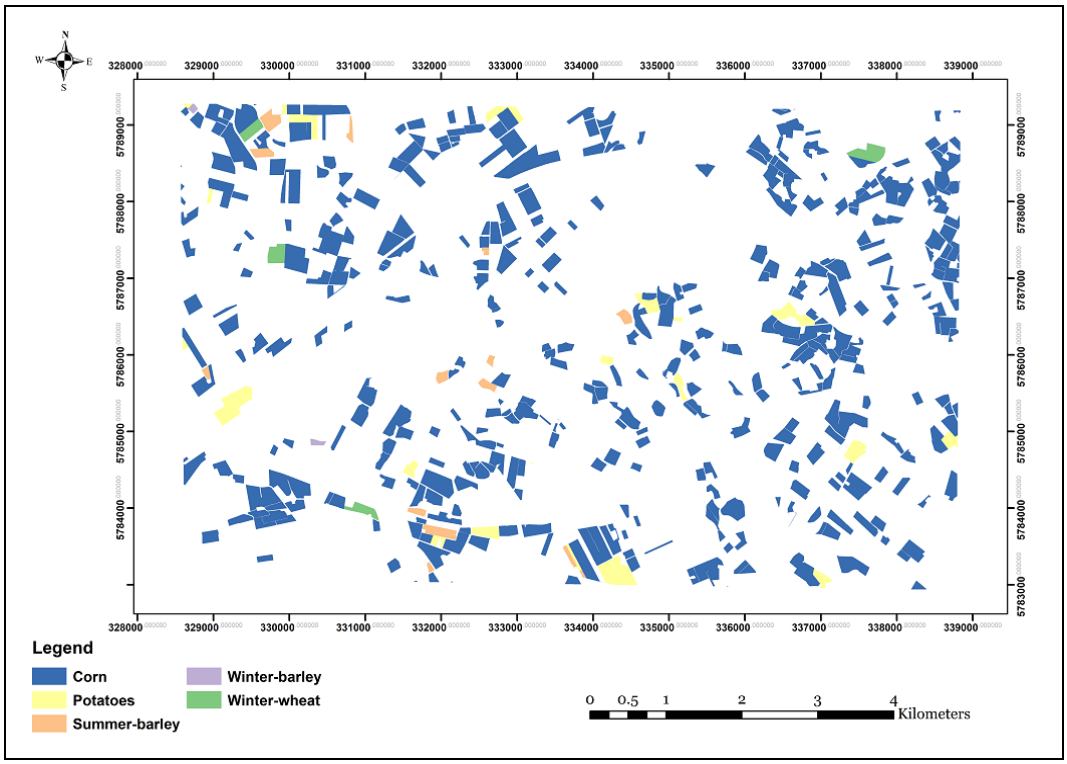

Figure 6: Crop type map generated from data obtained from the Dutch National georegister

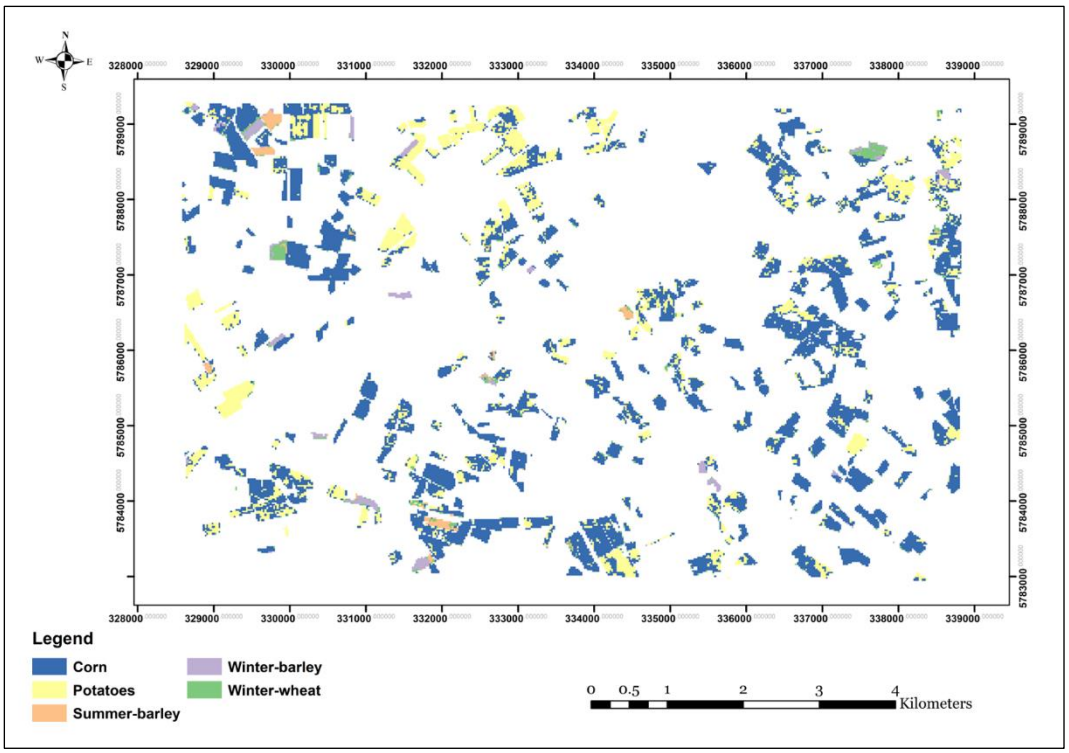

Figure 7: Crop type map generated from the pixel-based classification (TWDTW) using PS images

5.2. Segmentation multi-temporal PS images

The segmentation applied using the parameters h = 0.05, nN =15 and 1000 iterations yielded the best results when visually compared with the agricultural plots. These parameters yielded the best

segmentation results while using single images and multiple images. Comparing segmentation results obtained using single images and multiple images, the multiple images one produced better segmentation results. Thus, segmentation using multiples images were adopted for this study (Figure 8). However, the left upper part of the study area showed larger segments compared to the lower and upper right area, which showed many small segments (over-segmentation). Over-segmentation is more preferred than under-segmentation (Yan and Roy, 2016; Csillik et al., 2019). Since over-segmentation is easier to correct than under-segmentation. The results of the segmentation agree with results obtained by Su et al. (2015) whereby the mean shift algorithm resulted in over-segmentation of the crop fields.

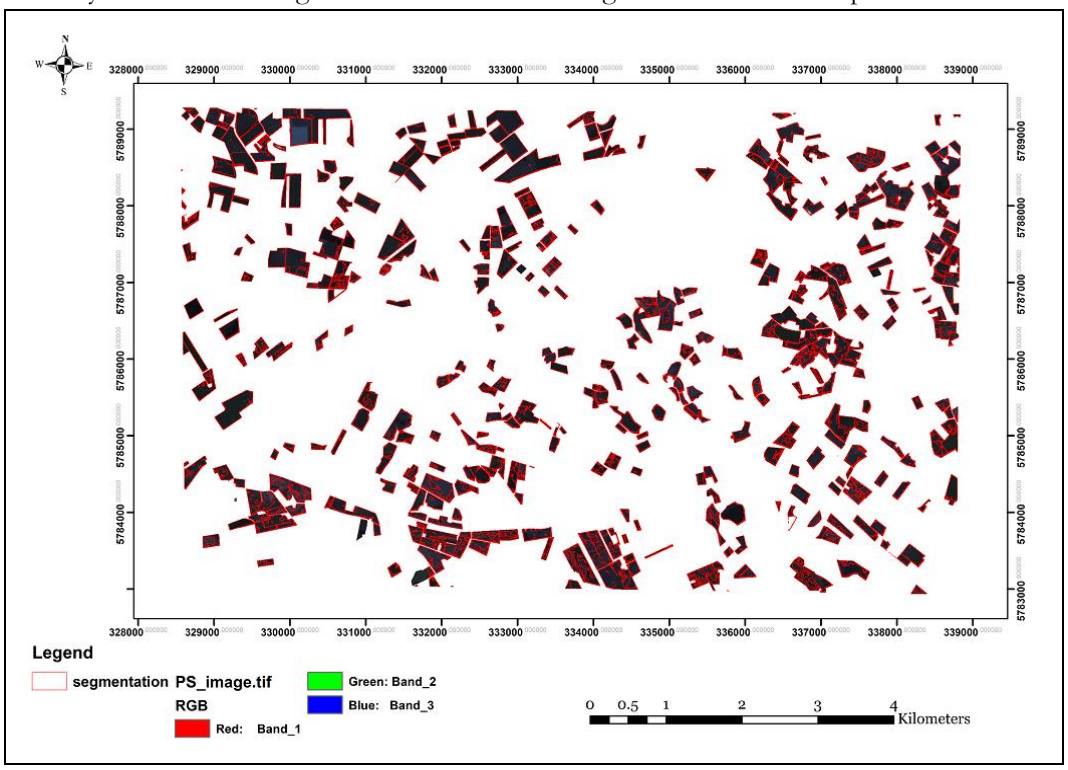

Figure 8: Mean shift segmentation results at h=0.05, nN= 15 and 1000 iterations for PS images

5.3. Object-based classification results using PS images

The resulting overall accuracy for object-based classification was 78.08%, as shown in Table 9. Corn recorded the highest UA with 88.89%, followed by summer barley at 88.24 %. Even though corn had confusion with potatoes (9 samples) and summer barley (2 samples), the confusion did not affect much the obtained user's accuracy since only a few samples were misclassified. Winter barley recorded the lowest user accuracy of 67.61% due to confusion with winter wheat. Combining winter wheat and winter barley to form winter grains resulted in UA of 90.11% and OA increase of 1.34% to 79.42%. The crop map obtained from the object-based classification is represented in Figure 9. The crop type map is more homogeneous than the one obtained by pixel-based classification. The homogeneity in the classification can be explained by the fact that objects were used as spatial input units for the classification (Belgiu and Csillik, 2018).

Table 9: Confusion matrix for object-based classification

	Corn	Potatoes	Summer barley	Winter barley	Winter wheat	Total	UA (%)
Corn	88	9	2	0	0	99	88.89
Potatoes	51	140	0	0	0	191	73.30
Summer barley	6	0	45	0	0	51	88.24
Winter barley	1	0	0	48	22	71	67.61
Winter wheat	3	0	2	2	28	35	80
Total	149	149	49	50	50	447	
PA (%)	59.06	93.96	91.84	96	56	**OA (%)**	**78.08**

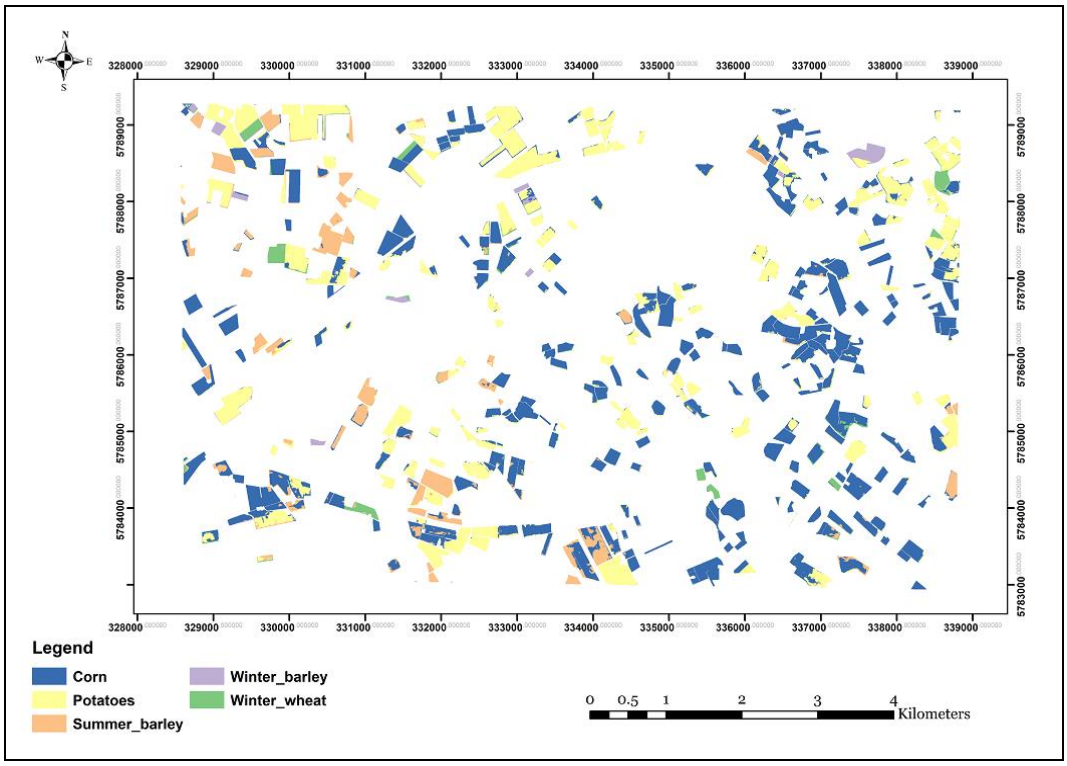

Figure 9: Crop type map generated from the object-based classification (tcDTW)

5.4. Comparing pixel-based and object-based classification

The study has evaluated the application of TWDTW (Maus et al., 2016) and tcDTW (Csillik et al., 2019) methods in mapping crops in smallholder farm systems in Diepenheim using PS NDVI time series data.
In comparing pixel-based and object-based classification, the used computers had the following configurations: server system (Intel(R) Xeon(R) CPU E5-2643v3 3.04GHz 3.39 GHz (2 processors) and 128 GB RAM generating 24 cores), used for the pixel-based classification and personal computer system (Intel(R) Core(TM) i7-8750H CPU @2.20GHz 2.21GHz (2 processors) and 16 GB RAM generating 12 cores) used for object-based classification. Although a more powerful computer (server) was used for processing in pixel-based classification, the process took 9.9 hours, whereas the object-based classification took 3 hours. These results are in agreement with the study done by Belgiu and Csillik, (2018), where

pixel-based classification took longer computational time than the object-based classification. Pixel-based classification took long because the classifier (TWDTW) analysis was applied to each of the pixels. The object-based classification was computationally more efficient (took less time) since tcDTW algorithm used objects as spatial inputs were fewer as compared with pixels.
Corn class recorded high UA for object-based classification at 88.89%, followed by summer barley at 88.24% (Table 10). There was a slight decrease of 0.95% for class potatoes UA from the one attained using pixel-based classification. Winter wheat remained at UA of 80% for both pixel and object-based classification, whereas, there was a decrease of 6.58% in UA when using object-based classification.
The object-based classification resulted in higher overall accuracy than the pixel-based classification. The results of the study were in agreement with the results of studies by Belgiu and Csillik (2018) and Castillejo-González et al. (2009).

Table 10: Comparison between classification accuracies of pixel-based and object-based classifications

	Corn		**Potatoes**		**Summer barley**		**Winter barley**		**Winter wheat**		
Classification	PA (%)	UA (%)	PA (%)	UA (%)	PA (%)	UA (%)	PA (%)	UA (%)	PA (%)	UA (%)	OA (%)
Pixel-based	72	76.06	82.7	74.25	62	79.49	92	74.19	64	80	**75.78**
Object-based	59.06	88.89	93.96	73.3	91.84	88.24	96	67.61	56	80	**78.08**

McNemar's Chi-square test was used to compare the classification results of TWDTW and tcDTW (Table 11). The chi-squared ($\chi 2$) of 6.12 and p-value of 0.0133 was calculated (Table 11). The resulting p-value was less than 0.05; hence, the conclusion that the classification results by TWDTW were statistically different from the classification results generated by tcDTW.

Table 11: Classification results comparison using McNemar's Chi-square test

Classifications		$\chi 2$	p-value
Pixel-based TWDTW	Object-based tcDTW	6.12	0.0133

Comparing the crop type classification maps, object-based classification (Figure 9) resulted in less noisy classification map than pixel-based (Figure 7) (Valero et al., 2016). The results were obtained in this study an indication that TWDTW and tcDTW can be used to map crops ins smallholder farm systems using PS images. However, the models did not achieve high classification accuracies as the one obtained by Belgiu and Csillik, (2018) (TWDTW) and Csillik et al. (2019) (tcDTW) since most cops showed similar spectral characteristics as shown by the temporal patterns (Figure 4)

5.5. Suitability of PS images to map crops in smallholder farm systems

The results realised after the evaluation of suitability of PS images to map crops in smallholder farms in terms of spatial, temporal and spectral resolutions are shown below:

5.5.1. Spatial resolution suitability of PS images to map crops in smallholder farm systems

The results of the segmentation evaluations show that the average maximum biggest sub-object after elimination of extra pixels is 82.61%, as shown in Table 12. This is an indication that there was over-segmentation. The percentage of lost pixels and extra pixels were recorded at 0% and 0.34% respectively for the evaluation result, which shows that there was minimal under segmentation in the segmentation of the PS images. Further, under segmentation can be evaluated by the number of lost pixels that exceeds

25% of the reference object. The assumption is that if over 25% pixels of the reference object is lost to the neighbouring object(s), then there is a possibility that the reference area will be distorted after segmentation which would affect its shape. Therefore the number of distorted reference objects can as well be used to show under segmentation. The results show that there was neither object lost nor deformed objects due to extra pixels. Segmentation evaluation results from PS images were compared with segmentation results from S2 images. Segmentation for S2 images was realised using parameters h=17, nN= 20 and 1000 h. The average maximum sub-object using S2 images was 83.04% and extra pixels at 0.77%, as shown in Table 12. Comparing the segmentation evaluation results between PS images and S2 images shows that the is minimal difference in in the results. Under-segmentation is minimal for both segmentation; hence the segmentation evaluation agrees with results obtained by Csillik et al. (2019).

Table 12: Segmentation evaluation results for mean shift segmentation

Criteria	**Results**	
	PS images	**S2 images**
Avg. % max Area:	82.61	83.04
Lost pixels (%):	0	0
Extra pixels (%):	0.34	0.77
No. of lost objects:	0	0
No. of deformed objects due to extra pixels:	0	0

5.5.2. Temporal resolution suitability of PS images to map crops in smallholder farm systems

Increasing PS images from the 11 images to 18 images lead to lower overall accuracy. The resulting OA of 54.89% (Table 13) was 20.89% less than the initial accuracy of 75.78% (Table 8). The results agree with the results obtained by Conrad et al. (2014) that showed that increasing the number of images may not lead to an increase in classification accuracy. Further, the results obtained from the classification contradicts Jain et al. (2016) argument that increasing the temporal frequency of the imagery will result in high classification accuracy. This study confirms that more images do not guarantee better classification output, but better classification results can be realised the use of optimal images per clop calendar (Conrad et al., 2014). Further, Meng et al. (2020) argued that optimal images to improve crop mapping classification could be realised by the use of middle and later stages of the growth cycle. However, multitemporal images increase the chances of obtaining cloud-free images.

Table 13: Confusion matrix for the NDVI time series from extra images

	Corn	**Potatoes**	**Summer barley**	**Winter barley**	**Winter wheat**	**Total**	**UA (%)**
Corn	51	33	5	0	0	89	57.30
Potatoes	95	117	7	0	0	219	53.42
Summer barley	3	0	35	0	17	55	63.64
Winter barley	1	0	2	16	5	24	66.67
Winter wheat	0	0	1	34	28	63	44.44
Total	150	150	50	50	50	450	
PA (%)	34	78	70	32	56	**OA (%)**	**54.89**

5.5.3. Spectral resolution suitability of PS images to map crops in smallholder farm systems

The results were obtained when TWDTW classifier parameters were set at alpha = -0.1 and beta = 90. For the classical NDVI, an OA of 58.67% was achieved, as presented in Figure 10. The tabular results for the classification accuracy assessment are presented in *appendices(Table 14-Table 24)*. The highest OA (74%) was achieved using $NDVI_{REA}1$ and the least using NDVIre with 32.44% (Figure 11). Using $NDVI_{REA}1$, the highest UA was recorded by winter barley 85.19%, followed by corn at 80.60% while winter wheat recorded lowest UA of 50.70% since it was confused with all the other classes.

Although $NDVI_{REA}2$ and $NDVI_{REA}4$ recorded lower OA than $NDVI_{REA}1$, they showed an improvement in OA from the one achieved from classical NDVI (Figure 10). Corn had the highest UA of 74.32% when using $NDVI_{REA}2$, whereas winter barley had the highest UA of 73.1% when using $NDVI_{REA}4$ (Figure 11). Corn sample showed high heterogeneity hence recording the lowest PA of 36.67% and 33.33% for $NDVI_{REA}2$ and $NDVI_{REA}4$ respectively.

Using $NDVI_{REA}3$, an OA 58.67% similar to the one realised using classical NDVI was recorded (Figure 10). However, higher UA was realised for classes summer barley (58.18%), winter barley (67.27%) and winter wheat (53.57%) with low UA recorded for classes corn and potatoes than when using classical NDVI where UAs for summer barley, winter barley and winter wheat were 56.67%, 59.62% and 44.44% respectively Figure 11.

The varied OA, UA and PA is an indication that NDVI from the red edge may lead to an improvement in accuracy. The accuracy improvement is class-specific based on the chlorophyll content in the leaves Schuster et al. (2012). This can be reflected in the results obtained using $NDVI_{REA}1$, which means band5 is more sensitive to crops than the other S2 bands used in the study.

Use of NDVIren1 resulted in OA of 58.00% (Figure 10), which was the highest classification accuracy for NDVIren and 0.67 % less than OA for classical NDVI. The UAs for summer barley, winter barley and winter wheat were higher than ones calculated from classical NDVI by 2.9%, 29.02% and 15.08% respectively (Figure 11). Using NDVIren2 for the classification, the OA reduced by 13.56% from 58.67 realised using classical NDVI to 45.11% (Figure 10). However, the UAs for potatoes and winter wheat increased by 3.7% and 32.03% respectively (Figure 11). Classification using NDVIren3 resulted in an OA, 2.67% lower than the one achieved through classical NDVI (Figure 10). The NDVIren3 resulted in increasing in UAs of summer barley, winter barley and winter wheat by 3.33%, 9.47 and 9.95% respectively (Figure 11). The results obtained using NDVIren1 and NDVIren3 concurs with the results obtained by Gerstmann et al. (2016), where they were able to distinguish between winter barley and winter wheat using red edge NDVI.

Classification using NDVIre resulted in OAs of 55.56%, 50.67%, 32.44% for NDVIre1, NDVIre2 and NDVIre3, respectively (Figure 10). These results (OAs) were lower than the one obtained using classical NDVI by 3.11% for NDVIre1, 8% for NDVIre2 and 26.23% for NDVIre3 (Figure 10). Only UA for winter barley was better than the one obtained using classical NDVI by 6.23% for NDVIre1. Similarly, for NDVIre2, only winter wheat had higher UA than the resulting one from classical NDVI by 19.92%.

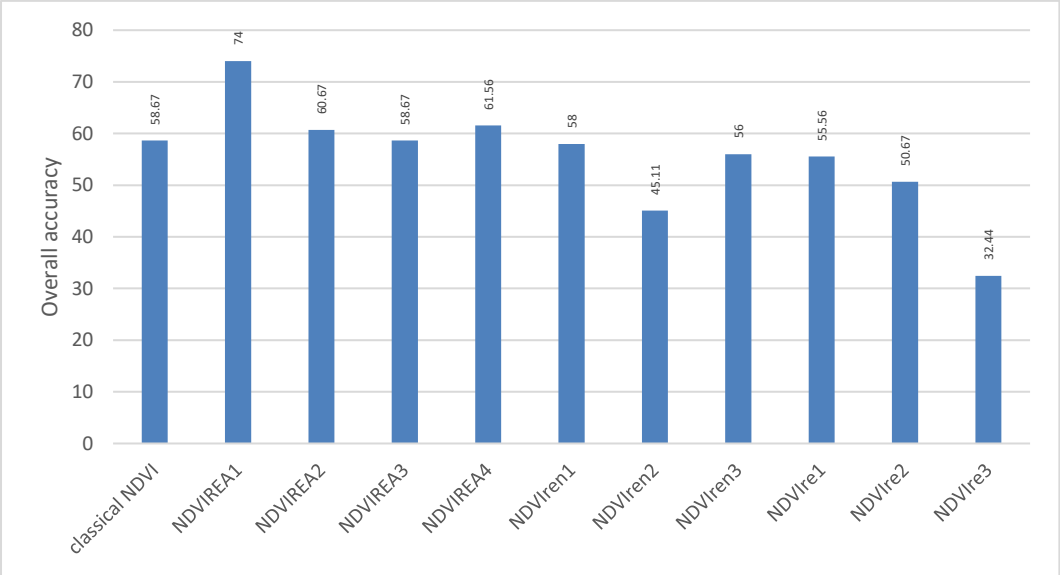

Figure 10: Comparison of OAs between classical NDVI and NDVI calculated using red edge bands

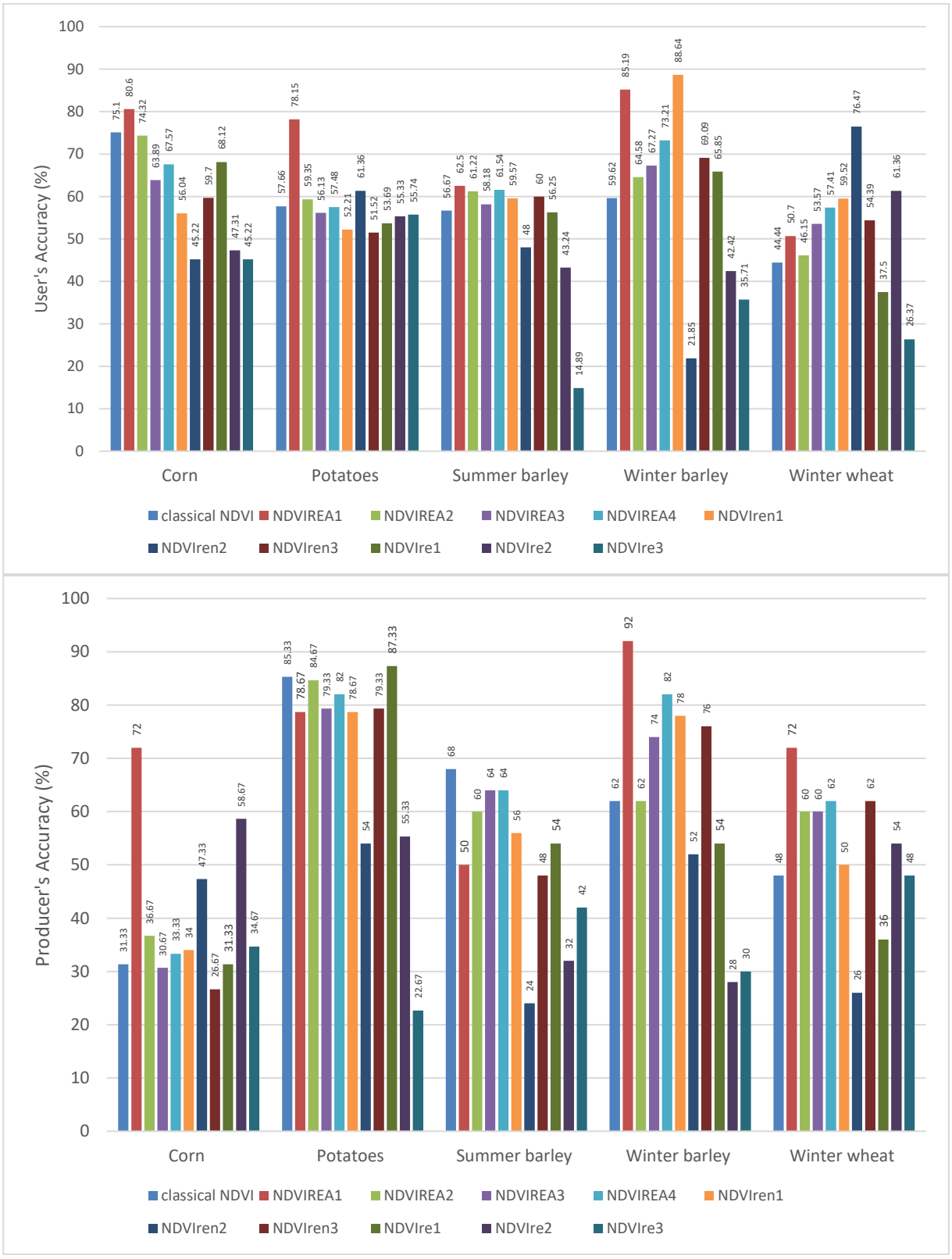

Figure 11: Summary of user's and producer's accuracies for classical NDVI and NDVI calculated using red edge bands

For results obtained using TWDTW to evaluate spectral suitability of PS images to map smallholder farms in Diepenheim using S2 red edge bands NDVI time series, band5 performed better than all the

other red edge bands within each category (NDVIren, NDVIre and $NDVI_{RE}$). The results obtained using $NDVI_{RE}$ were in agreement with Ustuner et al. (2014) results, which recorded higher classification accuracy when using the red-edge bands. Using NVDIre and NDVIren, the results obtained were on the contrary to the ones obtained by Sun et al. (2019) as they had lower overall accuracy than classical NDVI one.

6. CONCLUSION AND RECOMMENDATIONS

This chapter presents the conclusion, limitations of the study and recommendations for future study

6.1. Conclusion

The study made use of PS images to map crops in smallholder farm systems using multitemporal images and S2 images to evaluate the suitability of PS images to map smallholder farm systems. From the results obtained for the study, it can be concluded that:

- Object-based classification based on tcDTW took less time to compute than pixel-based classification using TWDTW.
- As well, object-based classification resulted in slightly higher OA (78.08%) than pixel-based classification with OA of 75.78%.
- The classification results generated using TWDTW and tcDTW classifiers were found to be significantly different using McNemar's Chi-square test.
- $NDVI_{REA}$ resulted in better classification results than classical NDVI when using band5 and band6, except when using band7. Thus, the use of $NDVI_{REA}$ improved crop type classification results
- NDVIren and NDVIre resulted in lower classification results than the classical NDVI hence did not improve classification results.

6.2. Study limitations

The study area did not exhibit heterogeneity like the ones exhibited in other smallholder farms such as the ones in Sub-Saharan Africa to be able to fully utilise the potential of the high spatial resolution of PS images to map crops in smallholder systems.

6.3. Recommendations

Similar future study may consider below recommendations:

- Study be done on a heterogeneous study area to fully exploit the high spatial resolution of PS images and its utility to map crops in smallholder farms
- The study can be implemented on a mixed cropping agricultural landscape.

LIST OF REFERENCES

Aguilar, R., Zurita-Milla, R., Izquierdo-Verdiguier, E., de By, R.A., 2018. A cloud-based multi-temporal ensemble classifier to map smallholder farming systems. Remote Sens. 10. https://doi.org/10.3390/rs10050729

Asgarian, A., Soffianian, A., Pourmanafi, S., 2016. Crop type mapping in a highly fragmented and heterogeneous agricultural landscape: A case of central Iran using multi-temporal Landsat 8 imagery. Comput. Electron. Agric. 127, 531–540. https://doi.org/10.1016/j.compag.2016.07.019

Ashourloo, D., Shahrabi, H.S., Azadbakht, M., Aghighi, H., Nematollahi, H., Alimohammadi, A., Matkan, A.A., 2019. Automatic canola mapping using time series of sentinel 2 images. ISPRS J. Photogramm. Remote Sens. 156, 63–76. https://doi.org/10.1016/j.isprsjprs.2019.08.007

Becker-Reshef, I., Justice, C., Sullivan, M., Vermote, E., Tucker, C., Anyamba, A., Small, J., Pak, E., Masuoka, E., Schmaltz, J., Hansen, M., Pittman, K., Birkett, C., Williams, D., Reynolds, C., Doorn, B., 2010. Monitoring Global Croplands with Coarse Resolution Earth Observations: The Global Agriculture Monitoring (GLAM) Project. Remote Sens. 2, 1589–1609. https://doi.org/10.3390/rs2061589

Belgiu, M., Csillik, O., 2018. Sentinel-2 cropland mapping using pixel-based and object-based time-weighted dynamic time warping analysis. Remote Sens. Environ. 204, 509–523. https://doi.org/10.1016/j.rse.2017.10.005

Breunig, F.M., Galvão, L.S., Dalagnol, R., Dauve, C.E., Parraga, A., Santi, A.L., Della Flora, D.P., Chen, S., 2020. Delineation of management zones in agricultural fields using cover–crop biomass estimates from PlanetScope data. Int. J. Appl. Earth Obs. Geoinf. 85, 102004. https://doi.org/10.1016/j.jag.2019.102004

Brink, A.V.A.N.D.E.N., 2004. Land Consolidation and the Emergence of the Metropolitan Landscape. FAO, LANDNET 1–10.

Brink, L. van den, Bus, C.B., Groten, J.A.M., Lotz, L.A.P., Timmer, R.D., Wiel, C. van de, 2008. Gewas- en teeltbeschrijving van suikerbiet, maïs en aardappel in relatie tot verspreiding van genetisch materiaal.

Castillejo-González, I.L., López-Granados, F., García-Ferrer, A., Peña-Barragán, J.M., Jurado-Expósito, M., de la Orden, M.S., González-Audicana, M., 2009. Object- and pixel-based analysis for mapping crops and their agro-environmental associated measures using QuickBird imagery. Comput. Electron. Agric. 68, 207–215. https://doi.org/10.1016/J.COMPAG.2009.06.004

Celik, Y.B., Sertel, E., Ustundag, B.B., 2015. Identification of corn and cotton fields using multi-temporal Spot6 NDVI data. 2015 4th Int. Conf. Agro-Geoinformatics, Agro-Geoinformatics 2015 23–26. https://doi.org/10.1109/Agro-Geoinformatics.2015.7248136

Chen, C.-F., Son, N.-T., Chen, C.-R., Cho, K., Hsiao, Y.-Y., Chiang, S.-H., Chang, L.-Y., 2015. Assessing rice crop damage and restoration using remote sensing in tsunami-affected areas, Japan. J. Appl. Remote Sens. 9, 096002. https://doi.org/10.1117/1.jrs.9.096002

Chen, Y., Lu, D., Moran, E., Batistella, M., Dutra, L.V., Sanches, I.D.A., da Silva, R.F.B., Huang, J., Luiz, A.J.B., de Oliveira, M.A.F., 2018. Mapping croplands, cropping patterns, and crop types using MODIS time-series data. Int. J. Appl. Earth Obs. Geoinf. 69, 133–147. https://doi.org/10.1016/j.jag.2018.03.005

Clinton, N., Holt, A., Scarborough, J., Yan, L.I., Gong, P., 2010. Accuracy assessment measures for object-based image segmentation goodness. Photogramm. Eng. Remote Sensing 76, 289–299. https://doi.org/10.14358/PERS.76.3.289

Comaniciu, D., Meer, P., 2002. Mean shift: A robust approach toward feature space analysis. IEEE Trans. Pattern Anal. Mach. Intell. 24, 603–619. https://doi.org/10.1109/34.1000236

Congalton, R.G., 2001. Accuracy assessment and validation of remotely sensed and other spatial information. Int. J. Wildl. Fire 10, 321–328. https://doi.org/10.1071/wf01031

Congalton, R.G., 1991. A review of assessing the accuracy of classifications of remotely sensed data. Remote Sens. Environ. 37, 35–46. https://doi.org/10.1016/0034-4257(91)90048-B

Conrad, C., Dech, S., Dubovyk, O., Fritsch, S., Klein, D., Löw, F., Schorcht, G., Zeidler, J., 2014. Derivation of temporal windows for accurate crop discrimination in heterogeneous croplands of Uzbekistan using multitemporal RapidEye images. Comput. Electron. Agric. 103, 63–74.

https://doi.org/10.1016/j.compag.2014.02.003
Csillik, O., Belgiu, M., Asner, G.P., Kelly, M., 2019. Object-based time-constrained dynamic time warping classification of crops using Sentinel-2. Remote Sens. 11. https://doi.org/10.3390/rs11101257
Darwinkel, A., 1997. Wintertarwe Teelthandleing NR 76 -Maart 1997.
Delrue, J., Bydekerke, L., Eerens, H., Gilliams, S., Piccard, I., Swinnen, E., 2013. Crop mapping in countries with small-scale farming: A case study for West Shewa, Ethiopia. Int. J. Remote Sens. 34, 2566–2582. https://doi.org/10.1080/01431161.2012.747016
Dong, Q., Chen, X., Chen, J., Zhang, C., Liu, L., Cao, X., Zang, Y., Zhu, X., Cui, X., 2020. Mapping Winter Wheat in North China Using Sentinel 2A / B Data : A Method Based on Phenology-Time Weighted Dynamic Time Warping. Remote Sens. 12.
Duro, D.C., Franklin, S.E., Dubé, M.G., 2012. A comparison of pixel-based and object-based image analysis with selected machine learning algorithms for the classification of agricultural landscapes using SPOT-5 HRG imagery. Remote Sens. Environ. 118, 259–272. https://doi.org/10.1016/j.rse.2011.11.020
EPSG, 2005. EPSG:28992: Amersfoort / RD New -- Netherlands - Holland- Dutch [WWW Document]. URL https://epsg.io/28992 (accessed 2.20.20).
Fernández-Manso, A., Fernández-Manso, O., Quintano, C., 2016. SENTINEL-2A red-edge spectral indices suitability for discriminating burn severity. Int. J. Appl. Earth Obs. Geoinf. 50, 170–175. https://doi.org/10.1016/j.jag.2016.03.005
Foerster, S., Kaden, K., Foerster, M., Itzerott, S., 2012. Crop type mapping using spectral-temporal profiles and phenological information. Comput. Electron. Agric. 89, 30–40. https://doi.org/10.1016/j.compag.2012.07.015
Foody, G.M., 2009. Sample size determination for image classification accuracy assessment and comparison. Int. J. Remote Sens. 30, 5273–5291. https://doi.org/10.1080/01431160903130937
Foody, G.M., Mathur, A., 2004. A relative evaluation of multiclass image classification by support vector machines. IEEE Trans. Geosci. Remote Sens. 42, 1335–1343. https://doi.org/10.1109/TGRS.2004.827257
Gao, X., Huete, A.R., Ni, W., Miura, T., 2000. Optical-biophysical relationships of vegetation spectra without background contamination. Remote Sens. Environ. 74, 609–620. https://doi.org/10.1016/S0034-4257(00)00150-4
Gerst - Wikipedia [WWW Document], n.d. URL https://nl.wikipedia.org/wiki/Gerst (accessed 5.30.20).
Gerstmann, H., Möller, M., Gläßer, C., 2016. Optimization of spectral indices and long-term separability analysis for classification of cereal crops using multi-spectral RapidEye imagery. Int. J. Appl. Earth Obs. Geoinf. 52, 115–125. https://doi.org/10.1016/j.jag.2016.06.001
Gitelson, A., Merzlyak, M.N., 1994. Spectral Reflectance Changes Associated with Autumn Senescence of Aesculus hippocastanum L. and Acer platanoides L. Leaves. Spectral Features and Relation to Chlorophyll Estimation. J. Plant Physiol. 143, 286–292. https://doi.org/10.1016/S0176-1617(11)81633-0
Gitelson, A.A., Merzlyak, M.N., 1997. Remote estimation of chlorophyll content in higher plant leaves. Int. J. Remote Sens. 18, 2691–2697. https://doi.org/10.1080/014311697217558
Guan, X., Huang, C., Liu, G., Meng, X., Liu, Q., 2016. Mapping Rice Cropping Systems in Vietnam Using an NDVI-Based Time-Series Similarity Measurement Based on DTW Distance. Remote Sens. 8, 19. https://doi.org/10.3390/rs8010019
Guan, X., Liu, G., Huang, C., Meng, X., Liu, Q., Wu, C., Ablat, X., Chen, Z., Wang, Q., 2018. An open-boundary locally weighted dynamic time warping method for cropland mapping. ISPRS Int. J. Geo-Information 7. https://doi.org/10.3390/ijgi7020075
Hennig, C., Meila, M., Murtagh, F., Rocci, R., 2015. Handbook of cluster analysis, CRC press. Taylor & Francis Group. https://doi.org/10.1201/b19706
Houborg, R., McCabe, M.F., 2016. High-Resolution NDVI from planet's constellation of earth observing nano-satellites: A new data source for precision agriculture. Remote Sens. 8. https://doi.org/10.3390/rs8090768
Inglada, J., Arias, M., Tardy, B., Hagolle, O., Valero, S., Morin, D., Dedieu, G., Sepulcre, G., Bontemps, S., Defourny, P., Koetz, B., 2015. Assessment of an operational system for crop type map production using high temporal and spatial resolution satellite optical imagery. Remote Sens. 7, 12356–12379. https://doi.org/10.3390/rs70912356

Jain, M., Mondal, P., Galford, G.L., Fiske, G., DeFries, R.S., 2017. An automated approach to map winter cropped area of smallholder farms across large scales using MODIS imagery. Remote Sens. 9. https://doi.org/10.3390/rs9060566

Jain, M., Srivastava, A.K., Balwinder-Singh, Joon, R.K., McDonald, A., Royal, K., Lisaius, M.C., Lobell, D.B., 2016. Mapping smallholder wheat yields and sowing dates using micro-satellite data. Remote Sens. 8, 860. https://doi.org/10.3390/rs8100860

Jantakat, Y., Juntakut, P., Plaiklang, S., Arree, W., Jantakat, C., 2019. Spatiotemporal change of urban agriculture using google earth imagery: A case of municipality of nakhonratchasima city, Thailand. Int. Arch. Photogramm. Remote Sens. Spat. Inf. Sci. - ISPRS Arch. 42, 1301–1306. https://doi.org/10.5194/isprs-archives-XLII-2-W13-1301-2019

Jin, Z., Azzari, G., Burke, M., Aston, S., Lobell, D.B., 2017. Mapping smallholder yield heterogeneity at multiple scales in eastern Africa. Remote Sens. 9. https://doi.org/10.3390/rs9090931

Jin, Z., Azzari, G., You, C., Di Tommaso, S., Aston, S., Burke, M., Lobell, D.B., 2019. Smallholder maize area and yield mapping at national scales with Google Earth Engine. Remote Sens. Environ. 228, 115–128. https://doi.org/10.1016/j.rse.2019.04.016

Kadaster, n.d. National geo register - PDOK [WWW Document]. URL https://www.nationaalgeoregister.nl/geonetwork/srv/dut/catalog.search#/metadata/b812a145-b4fe-4331-8dc6-d914327a87ff (accessed 3.18.20).

Lambert, M.J., Traoré, P.C.S., Blaes, X., Baret, P., Defourny, P., 2018. Estimating smallholder crops production at village level from Sentinel-2 time series in Mali's cotton belt. Remote Sens. Environ. 216, 647–657. https://doi.org/10.1016/j.rse.2018.06.036

Li, A., Liang, S., Wang, A., Qin, J., 2007. Estimating Crop Yield from Multi-temporal Satellite Data Using Multivariate Regression and Neural Network Techniques. Photogramm. Eng. Remote Sens. 73, 1149–1157. https://doi.org/10.14358/pers.73.10.1149

Li, M., Bijker, W., 2019. Vegetable classification in Indonesia using Dynamic Time Warping of Sentinel-1A dual polarization SAR time series. Int. J. Appl. Earth Obs. Geoinf. 78, 268–280. https://doi.org/10.1016/j.jag.2019.01.009

Liu, H., Dahlgren, R.A., Larsen, R.E., Devine, S.M., Roche, L.M., O' Geen, A.T., Wong, A.J.Y., Covello, S., Jin, Y., 2019. Estimating rangeland forage production using remote sensing data from a Small Unmanned Aerial System (sUAS) and planetscope satellite. Remote Sens. 11. https://doi.org/10.3390/rs11050595

Liu, M.W., Ozdogan, M., Zhu, X., 2014. Crop type classification by simultaneous use of satellite images of different resolutions. IEEE Trans. Geosci. Remote Sens. 52, 3637–3649. https://doi.org/10.1109/TGRS.2013.2274431

Lobell, D.B., Di Tommaso, S., You, C., Djima, I.Y., Burke, M., Kilic, T., 2020. Sight for sorghums: Comparisons of satellite-and ground-based sorghum yield estimates in Mali. Remote Sens. 12, 1–16. https://doi.org/10.3390/RS12010100

Lowder, S.K., Skoet, J., Raney, T., 2016. The Number, Size, and Distribution of Farms, Smallholder Farms, and Family Farms Worldwide. World Dev. 87, 16–29. https://doi.org/10.1016/j.worlddev.2015.10.041

Lu, D., Weng, Q., 2007. A survey of image classification methods and techniques for improving classification performance. Int. J. Remote Sens. 28, 823–870. https://doi.org/10.1080/01431160600746456

Lunetta, R.S., Balogh, M.E., 1999. Application of Multi-Temporal Landsat 5 TM Imagery for Wetland Identification. Photogramm. Eng. Remote Sensing, 65, 1303–1310.

Maass, K., 2013. Coping with the food and agriculture challenge: smallholder's agenda.Preparations and outcomes of the 2012 United Nations Conference on Sustainable Development (Rio+20). Food and Agriculture Organzation of the United Nations (2013).

Manabe, V.D., Melo, M.R.S., Rocha, J.V., 2018. Framework for mapping integrated crop-livestock systems in Mato Grosso, Brazil. Remote Sens. 10. https://doi.org/10.3390/rs10091322

Maponya, M.G., van Niekerk, A., Mashimbye, Z.E., 2020. Pre-harvest classification of crop types using a Sentinel-2 time-series and machine learning. Comput. Electron. Agric. 169, 105164. https://doi.org/10.1016/j.compag.2019.105164

Marpu, P.R., Neubert, M., Herold, H., Niemeyer, I., 2010. Enhanced evaluation of image segmentation results. J. Spat. Sci. 55, 55–68. https://doi.org/10.1080/14498596.2010.487850

Maus, V., Cˆ, G., Cartaxo, R., Sanchez, A., Ramos, F.M., Queiroz, R. De, 2016. A Time-Weighted Dynamic Time Warping method for land use and land cover mapping. IEEE J. Sel. Top. Appl. EARTH Obs. Remote Sens. XX, 1–12.

Maus, V., Câmara, G., Appel, M., Pebesma, E., 2019. **dtwSat** : Time-Weighted Dynamic Time Warping for Satellite Image Time Series Analysis in *R*. J. Stat. Softw. 88. https://doi.org/10.18637/jss.v088.i05

Maus, V., Camara, G., Cartaxo, R., Ramos, F.M., Sanchez, A., Ribeiro, G.Q., 2015. Open boundary dynamic time warping for satellite image time series classification. Int. Geosci. Remote Sens. Symp. 2015-Novem, 3349–3352. https://doi.org/10.1109/IGARSS.2015.7326536

McCarty, J.L., Neigh, C.S.R., Carroll, M.L., Wooten, M.R., 2017. Extracting smallholder cropped area in Tigray, Ethiopia with wall-to-wall sub-meter WorldView and moderate resolution Landsat 8 imagery. Remote Sens. Environ. 202, 142–151. https://doi.org/10.1016/j.rse.2017.06.040

McNemar, Q., 1947. Note on the sampling error of the difference between correlated proportions or percentages. Psychometrika 12, 153–157. https://doi.org/10.1007/BF02295996

Meng, S., Zhong, Y., Luo, C., Hu, X., Wang, X., Huang, S., 2020. Optimal temporal window selection for winter wheat and rapeseed mapping with Sentinel-2 Images: A case study of Zhongxiang in China. Remote Sens. 12. https://doi.org/10.3390/rs12020226

Mondal, S., Jeganathan, C., 2018. Mountain agriculture extraction from time-series MODIS NDVI using dynamic time warping technique. Int. J. Remote Sens. 39, 3679–3704. https://doi.org/10.1080/01431161.2018.1444289

Mtibaa, S., Irie, M., 2016. Land cover mapping in cropland dominated area using information on vegetation phenology and multi-seasonal Landsat 8 images. Euro-Mediterranean J. Environ. Integr. 1, 1–16. https://doi.org/10.1007/s41207-016-0006-5

Mudereri, B.T., Dube, T., Adel-Rahman, E.M., Niassy, S., Kimathi, E., Khan, Z., Landmann, T., 2019. A comparative analysis of planetscope and sentinel sentinel-2 space-borne sensors in mapping striga weed using guided regularised random forest classification ensemble, in: International Archives of the Photogrammetry, Remote Sensing and Spatial Information Sciences - ISPRS Archives. pp. 701–708. https://doi.org/10.5194/isprs-archives-XLII-2-W13-701-2019

Murthy, C.S., Raju, P. V., Badrinath, K.V.S., 2003. Classification of wheat crop with multi-temporal images: Performance of maximum likelihood and artificial neural networks. Int. J. Remote Sens. 24, 4871–4890. https://doi.org/10.1080/0143116031000070490

Neigh, C.S.R., Carroll, M.L., Wooten, M.R., McCarty, J.L., Powell, B.F., Husak, G.J., Enenkel, M., Hain, C.R., 2018. Smallholder crop area mapped with wall-to-wall WorldView sub-meter panchromatic image texture: A test case for Tigray, Ethiopia. Remote Sens. Environ. 212, 8–20. https://doi.org/10.1016/j.rse.2018.04.025

Netzel, P., Stepinski, T., 2018. Climate similarity search: Geoweb tool for exploring climate variability. Bull. Am. Meteorol. Soc. 99, 475–477. https://doi.org/10.1175/BAMS-D-16-0334.1

Odagawa, S., Seguchi, D., Okumura, T., 2019. Stability Estimation of a Sample Size for Interannual Monitoring Using Micro Satellites. Int. Geosci. Remote Sens. Symp. 7278–7281. https://doi.org/10.1109/IGARSS.2019.8899211

Ouzemou, J.E., El Harti, A., Lhissou, R., El Moujahid, A., Bouch, N., El Ouazzani, R., Bachaoui, E.M., El Ghmari, A., 2018. Crop type mapping from pansharpened Landsat 8 NDVI data: A case of a highly fragmented and intensive agricultural system. Remote Sens. Appl. Soc. Environ. 11, 94–103. https://doi.org/10.1016/j.rsase.2018.05.002

Ozdarici-Ok, A., Akyurek, Z., 2014. Object-based classification of multi-temporal images for agricultural crop mapping in Karacabey Plain, Turkey. Int. Arch. Photogramm. Remote Sens. Spat. Inf. Sci. - ISPRS Arch. 40, 127–132. https://doi.org/10.5194/isprsarchives-XL-7-127-2014

Pan, Z., Huang, J., Zhou, Q., Wang, L., Cheng, Y., Zhang, H., Blackburn, G.A., Yan, J., Liu, J., 2015. Mapping crop phenology using NDVI time-series derived from HJ-1 A/B data. Int. J. Appl. Earth Obs. Geoinf. 34, 188–197. https://doi.org/10.1016/j.jag.2014.08.011

Persello, C., Tolpekin, V.A., Bergado, J.R., de By, R.A., 2019. Delineation of agricultural fields in smallholder farms from satellite images using fully convolutional networks and combinatorial grouping. Remote Sens. Environ. 231. https://doi.org/10.1016/j.rse.2019.111253

Petitjean, F., Inglada, J., Gançarski, P., 2012. Satellite image time series analysis under time warping. IEEE Trans. Geosci. Remote Sens. 50, 3081–3095. https://doi.org/10.1109/TGRS.2011.2179050

Planet, P.I., 2019. Satellite Imagery and Archive | Planet [WWW Document]. URL https://www.planet.com/products/planet-imagery/ (accessed 6.13.19).

Potato - Wikipedia [WWW Document], n.d. URL https://nl.wikipedia.org/wiki/Aardappel (accessed 5.30.20).

Robertson, L.D., King, D.J., 2011. Comparison of pixel-and object-based classification in land cover change mapping. Int. J. Remote Sens. 32, 1505–1529. https://doi.org/10.1080/01431160903571791

Rouse, J.W., Hass, R.H., Schell, J.A., Deering, D.W., 1973. Monitoring vegetation systems in the great plains with ERTS. Third Earth Resour. Technol. Satell. Symp. 1, 309–317. https://doi.org/citeulike-article-id:12009708

Sakoe, H., Chiba, S., 1978. Dynamic programming algorithm optimization for spoken word recognition. IEEE Trans. Acoust. 26, 43.

Schuster, C., Förster, M., Kleinschmit, B., 2012. Testing the red edge channel for improving land-use classifications based on high-resolution multi-spectral satellite data. Int. J. Remote Sens. 33, 5583–5599. https://doi.org/10.1080/01431161.2012.666812

Simoes, R., Pletsch, M., Santos, L., Câmara, G., Maus, V., 2017. Satellite multisensor spatiotemporal analysis: a TWDTW preview approach. Simpósio Bras. Sensoriamento Remoto 6943–6950.

Skakun, S., Franch, B., Vermote, E., Roger, J.C., Becker-Reshef, I., Justice, C., Kussul, N., 2017. Early season large-area winter crop mapping using MODIS NDVI data, growing degree days information and a Gaussian mixture model. Remote Sens. Environ. 195, 244–258. https://doi.org/10.1016/j.rse.2017.04.026

Su, T., Li, H., Zhang, S., Li, Y., 2015. Image segmentation using mean shift for extracting croplands from high-resolution remote sensing imagery. Remote Sens. Lett. 6, 952–961. https://doi.org/10.1080/2150704X.2015.1093188

Sun, C., Bian, Y., Zhou, T., Pan, J., 2019. Using of Multi-Source and Multi-Temporal Remote. Remote. Multi-temporal Reg. Subtrop. Agric. 19, 1–23.

Thapa, G., 2010. Smallholder or Family Farming in Transforming Economies of Asia, in: IFAD.

Turker, M., Arikan, M., 2005. Sequential masking classification of multi-temporal Landsat7 ETM+ images for field-based crop mapping in Karacabey, Turkey. Int. J. Remote Sens. 26, 3813–3830. https://doi.org/10.1080/01431160500166391

U.N. Dept. of Economic and Social Affairs, 2017. World population projected to reach 9.8 billion in 2050, and 11.2 billion in 2100 | UN DESA | United Nations Department of Economic and Social Affairs, United Nations Department of Economic and Social Affairs.

UN News Centre, 2015. UN adopts new Global Goals, charting sustainable development for people and planet by 2030 [WWW Document]. United Nations Dep. Econ. Soc. Aff. https://doi.org/10.1080/02513625.2015.1038080

UNCTAD, 2015. Commodities and development report, United nations conference on trade and development. https://doi.org/UNCTAD/SUC/2014/5

Ustuner, M., Sanli, F.B., Abdikan, S., Esetlili, M.T., Kurucu, Y., 2014. Crop type classification using vegetation indices of rapideye imagery. Int. Arch. Photogramm. Remote Sens. Spat. Inf. Sci. - ISPRS Arch. 40, 195–198. https://doi.org/10.5194/isprsarchives-XL-7-195-2014

Valero, S., Morin, D., Inglada, J., Sepulcre, G., Arias, M., Hagolle, O., Dedieu, G., Bontemps, S., Defourny, P., Koetz, B., 2016. Production of a dynamic cropland mask by processing remote sensing image series at high temporal and spatial resolutions. Remote Sens. 8, 1–21. https://doi.org/10.3390/rs8010055

Vuolo, F., Neuwirth, M., Immitzer, M., Atzberger, C., Ng, W.T., 2018. How much does multi-temporal Sentinel-2 data improve crop type classification? Int. J. Appl. Earth Obs. Geoinf. 72, 122–130. https://doi.org/10.1016/j.jag.2018.06.007

Wang, C., Chen, J., Wu, J., Tang, Y., Shi, P., Black, T.A., Zhu, K., 2017. A snow-free vegetation index for improved monitoring of vegetation spring green-up date in deciduous ecosystems. Remote Sens. Environ. 196, 1–12. https://doi.org/10.1016/j.rse.2017.04.031

Wardlow, B.D., Egbert, S.L., 2010. A comparison of MODIS 250-m EVI and NDVI data for crop mapping: A case study for southwest Kansas. Int. J. Remote Sens. 31, 805–830. https://doi.org/10.1080/01431160902897858

Wegner, L., Zwart, G., 2011. Who will feed the world? The production challenge, OXFAM. https://doi.org/10.3362/2046-1887.2011.017

Wood, S.N., 2017. Generalized Additive Models An Introduction with R SECOND EDITION, CRC press. Taylor & Francis Group, LLC. https://doi.org/10.1214/ss/1177013609

Wood, S.N., 2011. Fast stable restricted maximum likelihood and marginal likelihood estimation of semiparametric generalized linear models. J. R. Stat. Soc. Ser. B Stat. Methodol. 73, 3–36. https://doi.org/10.1111/j.1467-9868.2010.00749.x

Wu, K.L., Yang, M.S., 2007. Mean shift-based clustering. Pattern Recognit. 40, 3035–3052. https://doi.org/10.1016/j.patcog.2007.02.006

Xiao, X., Boles, S., Liu, J., Zhuang, D., Frolking, S., Li, C., Salas, W., Moore, B., 2005. Mapping paddy rice agriculture in southern China using multi-temporal MODIS images. Remote Sens. Environ. 95, 480–492. https://doi.org/10.1016/j.rse.2004.12.009

Xie, B., Zhang, H.K., Xue, J., 2019. Deep convolutional neural network for mapping smallholder agriculture using high spatial resolution satellite image. Sensors (Switzerland) 19. https://doi.org/10.3390/s19102398

Xie, Q., Dash, J., Huang, W., Peng, D., Qin, Q., Mortimer, H., Casa, R., Pignatti, S., Laneve, G., Pascucci, S., Dong, Y., Ye, H., 2018. Vegetation Indices Combining the Red and Red-Edge Spectral Information for Leaf Area Index Retrieval. IEEE J. Sel. Top. Appl. Earth Obs. Remote Sens. 11, 1482–1492. https://doi.org/10.1109/JSTARS.2018.2813281

Xu, L., Ming, D., Zhou, W., Bao, H., Chen, Y., Ling, X., 2019. Farmland extraction from high spatial resolution remote sensing images based on stratified scale pre-estimation. Remote Sens. 11. https://doi.org/10.3390/rs11020108

Zhang, J., Wang, R., Xie, C., Xie, J., Fu, K., 2013. An algorithm for segmenting pest from crop pest image with complicated background. J. Comput. Inf. Syst. 9, 3857–3864. https://doi.org/10.12733/jcis5818

Zheng, B., Myint, S.W., Thenkabail, P.S., Aggarwal, R.M., 2015. A support vector machine to identify irrigated crop types using time-series Landsat NDVI data. Int. J. Appl. Earth Obs. Geoinf. 34, 103–112. https://doi.org/10.1016/j.jag.2014.07.002

Aguilar, R., Zurita-Milla, R., Izquierdo-Verdiguier, E., de By, R.A., 2018. A cloud-based multi-temporal ensemble classifier to map smallholder farming systems. Remote Sens. 10. https://doi.org/10.3390/rs10050729

Asgarian, A., Soffianian, A., Pourmanafi, S., 2016. Crop type mapping in a highly fragmented and heterogeneous agricultural landscape: A case of central Iran using multi-temporal Landsat 8 imagery. Comput. Electron. Agric. 127, 531–540. https://doi.org/10.1016/j.compag.2016.07.019

Ashourloo, D., Shahrabi, H.S., Azadbakht, M., Aghighi, H., Nematollahi, H., Alimohammadi, A., Matkan, A.A., 2019. Automatic canola mapping using time series of sentinel 2 images. ISPRS J. Photogramm. Remote Sens. 156, 63–76. https://doi.org/10.1016/j.isprsjprs.2019.08.007

Becker-Reshef, I., Justice, C., Sullivan, M., Vermote, E., Tucker, C., Anyamba, A., Small, J., Pak, E., Masuoka, E., Schmaltz, J., Hansen, M., Pittman, K., Birkett, C., Williams, D., Reynolds, C., Doorn, B., 2010. Monitoring Global Croplands with Coarse Resolution Earth Observations: The Global Agriculture Monitoring (GLAM) Project. Remote Sens. 2, 1589–1609. https://doi.org/10.3390/rs2061589

Belgiu, M., Csillik, O., 2018. Sentinel-2 cropland mapping using pixel-based and object-based time-weighted dynamic time warping analysis. Remote Sens. Environ. 204, 509–523. https://doi.org/10.1016/j.rse.2017.10.005

Breunig, F.M., Galvão, L.S., Dalagnol, R., Dauve, C.E., Parraga, A., Santi, A.L., Della Flora, D.P., Chen, S., 2020. Delineation of management zones in agricultural fields using cover–crop biomass estimates from PlanetScope data. Int. J. Appl. Earth Obs. Geoinf. 85, 102004. https://doi.org/10.1016/j.jag.2019.102004

Brink, A.V.A.N.D.E.N., 2004. Land Consolidation and the Emergence of the Metropolitan Landscape. FAO, LANDNET 1–10.

Brink, L. van den, Bus, C.B., Groten, J.A.M., Lotz, L.A.P., Timmer, R.D., Wiel, C. van de, 2008. Gewas- en teeltbeschrijving van suikerbiet, maïs en aardappel in relatie tot verspreiding van genetisch materiaal.

Castillejo-González, I.L., López-Granados, F., García-Ferrer, A., Peña-Barragán, J.M., Jurado-Expósito, M., de la Orden, M.S., González-Audicana, M., 2009. Object- and pixel-based analysis for mapping crops and their agro-environmental associated measures using QuickBird imagery. Comput.

Electron. Agric. 68, 207–215. https://doi.org/10.1016/J.COMPAG.2009.06.004
Celik, Y.B., Sertel, E., Ustundag, B.B., 2015. Identification of corn and cotton fields using multi-temporal Spot6 NDVI data. 2015 4th Int. Conf. Agro-Geoinformatics, Agro-Geoinformatics 2015 23–26. https://doi.org/10.1109/Agro-Geoinformatics.2015.7248136
Chen, C.-F., Son, N.-T., Chen, C.-R., Cho, K., Hsiao, Y.-Y., Chiang, S.-H., Chang, L.-Y., 2015. Assessing rice crop damage and restoration using remote sensing in tsunami-affected areas, Japan. J. Appl. Remote Sens. 9, 096002. https://doi.org/10.1117/1.jrs.9.096002
Chen, Y., Lu, D., Moran, E., Batistella, M., Dutra, L.V., Sanches, I.D.A., da Silva, R.F.B., Huang, J., Luiz, A.J.B., de Oliveira, M.A.F., 2018. Mapping croplands, cropping patterns, and crop types using MODIS time-series data. Int. J. Appl. Earth Obs. Geoinf. 69, 133–147. https://doi.org/10.1016/j.jag.2018.03.005
Clinton, N., Holt, A., Scarborough, J., Yan, L.I., Gong, P., 2010. Accuracy assessment measures for object-based image segmentation goodness. Photogramm. Eng. Remote Sensing 76, 289–299. https://doi.org/10.14358/PERS.76.3.289
Comaniciu, D., Meer, P., 2002. Mean shift: A robust approach toward feature space analysis. IEEE Trans. Pattern Anal. Mach. Intell. 24, 603–619. https://doi.org/10.1109/34.1000236
Congalton, R.G., 2001. Accuracy assessment and validation of remotely sensed and other spatial information. Int. J. Wildl. Fire 10, 321–328. https://doi.org/10.1071/wf01031
Congalton, R.G., 1991. A review of assessing the accuracy of classifications of remotely sensed data. Remote Sens. Environ. 37, 35–46. https://doi.org/10.1016/0034-4257(91)90048-B
Conrad, C., Dech, S., Dubovyk, O., Fritsch, S., Klein, D., Löw, F., Schorcht, G., Zeidler, J., 2014. Derivation of temporal windows for accurate crop discrimination in heterogeneous croplands of Uzbekistan using multitemporal RapidEye images. Comput. Electron. Agric. 103, 63–74. https://doi.org/10.1016/j.compag.2014.02.003
Csillik, O., Belgiu, M., Asner, G.P., Kelly, M., 2019. Object-based time-constrained dynamic time warping classification of crops using Sentinel-2. Remote Sens. 11. https://doi.org/10.3390/rs11101257
Darwinkel, A., 1997. Wintertarwe Teelthandleing NR 76 -Maart 1997.
Delrue, J., Bydekerke, L., Eerens, H., Gilliams, S., Piccard, I., Swinnen, E., 2013. Crop mapping in countries with small-scale farming: A case study for West Shewa, Ethiopia. Int. J. Remote Sens. 34, 2566–2582. https://doi.org/10.1080/01431161.2012.747016
Dong, Q., Chen, X., Chen, J., Zhang, C., Liu, L., Cao, X., Zang, Y., Zhu, X., Cui, X., 2020. Mapping Winter Wheat in North China Using Sentinel 2A / B Data : A Method Based on Phenology-Time Weighted Dynamic Time Warping. Remote Sens. 12.
Duro, D.C., Franklin, S.E., Dubé, M.G., 2012. A comparison of pixel-based and object-based image analysis with selected machine learning algorithms for the classification of agricultural landscapes using SPOT-5 HRG imagery. Remote Sens. Environ. 118, 259–272. https://doi.org/10.1016/j.rse.2011.11.020
EPSG, 2005. EPSG:28992: Amersfoort / RD New -- Netherlands - Holland- Dutch [WWW Document]. URL https://epsg.io/28992 (accessed 2.20.20).
Fernández-Manso, A., Fernández-Manso, O., Quintano, C., 2016. SENTINEL-2A red-edge spectral indices suitability for discriminating burn severity. Int. J. Appl. Earth Obs. Geoinf. 50, 170–175. https://doi.org/10.1016/j.jag.2016.03.005
Foerster, S., Kaden, K., Foerster, M., Itzerott, S., 2012. Crop type mapping using spectral-temporal profiles and phenological information. Comput. Electron. Agric. 89, 30–40. https://doi.org/10.1016/j.compag.2012.07.015
Foody, G.M., 2009. Sample size determination for image classification accuracy assessment and comparison. Int. J. Remote Sens. 30, 5273–5291. https://doi.org/10.1080/01431160903130937
Foody, G.M., Mathur, A., 2004. A relative evaluation of multiclass image classification by support vector machines. IEEE Trans. Geosci. Remote Sens. 42, 1335–1343. https://doi.org/10.1109/TGRS.2004.827257
Gao, X., Huete, A.R., Ni, W., Miura, T., 2000. Optical-biophysical relationships of vegetation spectra without background contamination. Remote Sens. Environ. 74, 609–620. https://doi.org/10.1016/S0034-4257(00)00150-4
Gerst - Wikipedia [WWW Document], n.d. URL https://nl.wikipedia.org/wiki/Gerst (accessed 5.30.20).
Gerstmann, H., Möller, M., Gläßer, C., 2016. Optimization of spectral indices and long-term separability

analysis for classification of cereal crops using multi-spectral RapidEye imagery. Int. J. Appl. Earth Obs. Geoinf. 52, 115–125. https://doi.org/10.1016/j.jag.2016.06.001

Gitelson, A., Merzlyak, M.N., 1994. Spectral Reflectance Changes Associated with Autumn Senescence of Aesculus hippocastanum L. and Acer platanoides L. Leaves. Spectral Features and Relation to Chlorophyll Estimation. J. Plant Physiol. 143, 286–292. https://doi.org/10.1016/S0176-1617(11)81633-0

Gitelson, A.A., Merzlyak, M.N., 1997. Remote estimation of chlorophyll content in higher plant leaves. Int. J. Remote Sens. 18, 2691–2697. https://doi.org/10.1080/014311697217558

Guan, X., Huang, C., Liu, G., Meng, X., Liu, Q., 2016. Mapping Rice Cropping Systems in Vietnam Using an NDVI-Based Time-Series Similarity Measurement Based on DTW Distance. Remote Sens. 8, 19. https://doi.org/10.3390/rs8010019

Guan, X., Liu, G., Huang, C., Meng, X., Liu, Q., Wu, C., Ablat, X., Chen, Z., Wang, Q., 2018. An open-boundary locally weighted dynamic time warping method for cropland mapping. ISPRS Int. J. Geo-Information 7. https://doi.org/10.3390/ijgi7020075

Hennig, C., Meila, M., Murtagh, F., Rocci, R., 2015. Handbook of cluster analysis, CRC press. Taylor & Francis Group. https://doi.org/10.1201/b19706

Houborg, R., McCabe, M.F., 2016. High-Resolution NDVI from planet's constellation of earth observing nano-satellites: A new data source for precision agriculture. Remote Sens. 8. https://doi.org/10.3390/rs8090768

Inglada, J., Arias, M., Tardy, B., Hagolle, O., Valero, S., Morin, D., Dedieu, G., Sepulcre, G., Bontemps, S., Defourny, P., Koetz, B., 2015. Assessment of an operational system for crop type map production using high temporal and spatial resolution satellite optical imagery. Remote Sens. 7, 12356–12379. https://doi.org/10.3390/rs70912356

Jain, M., Mondal, P., Galford, G.L., Fiske, G., DeFries, R.S., 2017. An automated approach to map winter cropped area of smallholder farms across large scales using MODIS imagery. Remote Sens. 9. https://doi.org/10.3390/rs9060566

Jain, M., Srivastava, A.K., Balwinder-Singh, Joon, R.K., McDonald, A., Royal, K., Lisaius, M.C., Lobell, D.B., 2016. Mapping smallholder wheat yields and sowing dates using micro-satellite data. Remote Sens. 8, 860. https://doi.org/10.3390/rs8100860

Jantakat, Y., Juntakut, P., Plaiklang, S., Arree, W., Jantakat, C., 2019. Spatiotemporal change of urban agriculture using google earth imagery: A case of municipality of nakhonratchasima city, Thailand. Int. Arch. Photogramm. Remote Sens. Spat. Inf. Sci. - ISPRS Arch. 42, 1301–1306. https://doi.org/10.5194/isprs-archives-XLII-2-W13-1301-2019

Jin, Z., Azzari, G., Burke, M., Aston, S., Lobell, D.B., 2017. Mapping smallholder yield heterogeneity at multiple scales in eastern Africa. Remote Sens. 9. https://doi.org/10.3390/rs9090931

Jin, Z., Azzari, G., You, C., Di Tommaso, S., Aston, S., Burke, M., Lobell, D.B., 2019. Smallholder maize area and yield mapping at national scales with Google Earth Engine. Remote Sens. Environ. 228, 115–128. https://doi.org/10.1016/j.rse.2019.04.016

Kadaster, n.d. National geo register - PDOK [WWW Document]. URL https://www.nationaalgeoregister.nl/geonetwork/srv/dut/catalog.search#/metadata/b812a145-b4fe-4331-8dc6-d914327a87ff (accessed 3.18.20).

Lambert, M.J., Traoré, P.C.S., Blaes, X., Baret, P., Defourny, P., 2018. Estimating smallholder crops production at village level from Sentinel-2 time series in Mali's cotton belt. Remote Sens. Environ. 216, 647–657. https://doi.org/10.1016/j.rse.2018.06.036

Li, A., Liang, S., Wang, A., Qin, J., 2007. Estimating Crop Yield from Multi-temporal Satellite Data Using Multivariate Regression and Neural Network Techniques. Photogramm. Eng. Remote Sens. 73, 1149–1157. https://doi.org/10.14358/pers.73.10.1149

Li, M., Bijker, W., 2019. Vegetable classification in Indonesia using Dynamic Time Warping of Sentinel-1A dual polarization SAR time series. Int. J. Appl. Earth Obs. Geoinf. 78, 268–280. https://doi.org/10.1016/j.jag.2019.01.009

Liu, H., Dahlgren, R.A., Larsen, R.E., Devine, S.M., Roche, L.M., O' Geen, A.T., Wong, A.J.Y., Covello, S., Jin, Y., 2019. Estimating rangeland forage production using remote sensing data from a Small Unmanned Aerial System (sUAS) and planetscope satellite. Remote Sens. 11. https://doi.org/10.3390/rs11050595

Liu, M.W., Ozdogan, M., Zhu, X., 2014. Crop type classification by simultaneous use of satellite images of

different resolutions. IEEE Trans. Geosci. Remote Sens. 52, 3637–3649. https://doi.org/10.1109/TGRS.2013.2274431

Lobell, D.B., Di Tommaso, S., You, C., Djima, I.Y., Burke, M., Kilic, T., 2020. Sight for sorghums: Comparisons of satellite-and ground-based sorghum yield estimates in Mali. Remote Sens. 12, 1–16. https://doi.org/10.3390/RS12010100

Lowder, S.K., Skoet, J., Raney, T., 2016. The Number, Size, and Distribution of Farms, Smallholder Farms, and Family Farms Worldwide. World Dev. 87, 16–29. https://doi.org/10.1016/j.worlddev.2015.10.041

Lu, D., Weng, Q., 2007. A survey of image classification methods and techniques for improving classification performance. Int. J. Remote Sens. 28, 823–870. https://doi.org/10.1080/01431160600746456

Lunetta, R.S., Balogh, M.E., 1999. Application of Multi-Temporal Landsat 5 TM Imagery for Wetland Identification. Photogramm. Eng. Remote Sensing, 65, 1303–1310.

Maass, K., 2013. Coping with the food and agriculture challenge: smallholder's agenda.Preparations and outcomes of the 2012 United Nations Conference on Sustainable Development (Rio+20). Food and Agriculture Organzation of the United Nations (2013).

Manabe, V.D., Melo, M.R.S., Rocha, J.V., 2018. Framework for mapping integrated crop-livestock systems in Mato Grosso, Brazil. Remote Sens. 10. https://doi.org/10.3390/rs10091322

Maponya, M.G., van Niekerk, A., Mashimbye, Z.E., 2020. Pre-harvest classification of crop types using a Sentinel-2 time-series and machine learning. Comput. Electron. Agric. 169, 105164. https://doi.org/10.1016/j.compag.2019.105164

Marpu, P.R., Neubert, M., Herold, H., Niemeyer, I., 2010. Enhanced evaluation of image segmentation results. J. Spat. Sci. 55, 55–68. https://doi.org/10.1080/14498596.2010.487850

Maus, V., Cˆ, G., Cartaxo, R., Sanchez, A., Ramos, F.M., Queiroz, R. De, 2016. A Time-Weighted Dynamic Time Warping method for land use and land cover mapping. IEEE J. Sel. Top. Appl. EARTH Obs. Remote Sens. XX, 1–12.

Maus, V., Câmara, G., Appel, M., Pebesma, E., 2019. **dtwSat** : Time-Weighted Dynamic Time Warping for Satellite Image Time Series Analysis in *R*. J. Stat. Softw. 88. https://doi.org/10.18637/jss.v088.i05

Maus, V., Camara, G., Cartaxo, R., Ramos, F.M., Sanchez, A., Ribeiro, G.Q., 2015. Open boundary dynamic time warping for satellite image time series classification. Int. Geosci. Remote Sens. Symp. 2015-Novem, 3349–3352. https://doi.org/10.1109/IGARSS.2015.7326536

McCarty, J.L., Neigh, C.S.R., Carroll, M.L., Wooten, M.R., 2017. Extracting smallholder cropped area in Tigray, Ethiopia with wall-to-wall sub-meter WorldView and moderate resolution Landsat 8 imagery. Remote Sens. Environ. 202, 142–151. https://doi.org/10.1016/j.rse.2017.06.040

McNemar, Q., 1947. Note on the sampling error of the difference between correlated proportions or percentages. Psychometrika 12, 153–157. https://doi.org/10.1007/BF02295996

Meng, S., Zhong, Y., Luo, C., Hu, X., Wang, X., Huang, S., 2020. Optimal temporal window selection for winter wheat and rapeseed mapping with Sentinel-2 Images: A case study of Zhongxiang in China. Remote Sens. 12. https://doi.org/10.3390/rs12020226

Mondal, S., Jeganathan, C., 2018. Mountain agriculture extraction from time-series MODIS NDVI using dynamic time warping technique. Int. J. Remote Sens. 39, 3679–3704. https://doi.org/10.1080/01431161.2018.1444289

Mtibaa, S., Irie, M., 2016. Land cover mapping in cropland dominated area using information on vegetation phenology and multi-seasonal Landsat 8 images. Euro-Mediterranean J. Environ. Integr. 1, 1–16. https://doi.org/10.1007/s41207-016-0006-5

Mudereri, B.T., Dube, T., Adel-Rahman, E.M., Niassy, S., Kimathi, E., Khan, Z., Landmann, T., 2019. A comparative analysis of planetscope and sentinel sentinel-2 space-borne sensors in mapping striga weed using guided regularised random forest classification ensemble, in: International Archives of the Photogrammetry, Remote Sensing and Spatial Information Sciences - ISPRS Archives. pp. 701–708. https://doi.org/10.5194/isprs-archives-XLII-2-W13-701-2019

Murthy, C.S., Raju, P. V., Badrinath, K.V.S., 2003. Classification of wheat crop with multi-temporal images: Performance of maximum likelihood and artificial neural networks. Int. J. Remote Sens. 24, 4871–4890. https://doi.org/10.1080/0143116031000070490

Neigh, C.S.R., Carroll, M.L., Wooten, M.R., McCarty, J.L., Powell, B.F., Husak, G.J., Enenkel, M., Hain,

C.R., 2018. Smallholder crop area mapped with wall-to-wall WorldView sub-meter panchromatic image texture: A test case for Tigray, Ethiopia. Remote Sens. Environ. 212, 8–20. https://doi.org/10.1016/j.rse.2018.04.025

Netzel, P., Stepinski, T., 2018. Climate similarity search: Geoweb tool for exploring climate variability. Bull. Am. Meteorol. Soc. 99, 475–477. https://doi.org/10.1175/BAMS-D-16-0334.1

Odagawa, S., Seguchi, D., Okumura, T., 2019. Stability Estimation of a Sample Size for Interannual Monitoring Using Micro Satellites. Int. Geosci. Remote Sens. Symp. 7278–7281. https://doi.org/10.1109/IGARSS.2019.8899211

Ouzemou, J.E., El Harti, A., Lhissou, R., El Moujahid, A., Bouch, N., El Ouazzani, R., Bachaoui, E.M., El Ghmari, A., 2018. Crop type mapping from pansharpened Landsat 8 NDVI data: A case of a highly fragmented and intensive agricultural system. Remote Sens. Appl. Soc. Environ. 11, 94–103. https://doi.org/10.1016/j.rsase.2018.05.002

Ozdarici-Ok, A., Akyurek, Z., 2014. Object-based classification of multi-temporal images for agricultural crop mapping in Karacabey Plain, Turkey. Int. Arch. Photogramm. Remote Sens. Spat. Inf. Sci. - ISPRS Arch. 40, 127–132. https://doi.org/10.5194/isprsarchives-XL-7-127-2014

Pan, Z., Huang, J., Zhou, Q., Wang, L., Cheng, Y., Zhang, H., Blackburn, G.A., Yan, J., Liu, J., 2015. Mapping crop phenology using NDVI time-series derived from HJ-1 A/B data. Int. J. Appl. Earth Obs. Geoinf. 34, 188–197. https://doi.org/10.1016/j.jag.2014.08.011

Persello, C., Tolpekin, V.A., Bergado, J.R., de By, R.A., 2019. Delineation of agricultural fields in smallholder farms from satellite images using fully convolutional networks and combinatorial grouping. Remote Sens. Environ. 231. https://doi.org/10.1016/j.rse.2019.111253

Petitjean, F., Inglada, J., Gançarski, P., 2012. Satellite image time series analysis under time warping. IEEE Trans. Geosci. Remote Sens. 50, 3081–3095. https://doi.org/10.1109/TGRS.2011.2179050

Planet, P.I., 2019. Satellite Imagery and Archive | Planet [WWW Document]. URL https://www.planet.com/products/planet-imagery/ (accessed 6.13.19).

Potato - Wikipedia [WWW Document], n.d. URL https://nl.wikipedia.org/wiki/Aardappel (accessed 5.30.20).

Robertson, L.D., King, D.J., 2011. Comparison of pixel-and object-based classification in land cover change mapping. Int. J. Remote Sens. 32, 1505–1529. https://doi.org/10.1080/01431160903571791

Rouse, J.W., Hass, R.H., Schell, J.A., Deering, D.W., 1973. Monitoring vegetation systems in the great plains with ERTS. Third Earth Resour. Technol. Satell. Symp. 1, 309–317. https://doi.org/citeulike-article-id:12009708

Sakoe, H., Chiba, S., 1978. Dynamic programming algorithm optimization for spoken word recognition. IEEE Trans. Acoust. 26, 43.

Schuster, C., Förster, M., Kleinschmit, B., 2012. Testing the red edge channel for improving land-use classifications based on high-resolution multi-spectral satellite data. Int. J. Remote Sens. 33, 5583–5599. https://doi.org/10.1080/01431161.2012.666812

Simoes, R., Pletsch, M., Santos, L., Câmara, G., Maus, V., 2017. Satellite multisensor spatiotemporal analysis: a TWDTW preview approach. Simpósio Bras. Sensoriamento Remoto 6943–6950.

Skakun, S., Franch, B., Vermote, E., Roger, J.C., Becker-Reshef, I., Justice, C., Kussul, N., 2017. Early season large-area winter crop mapping using MODIS NDVI data, growing degree days information and a Gaussian mixture model. Remote Sens. Environ. 195, 244–258. https://doi.org/10.1016/j.rse.2017.04.026

Su, T., Li, H., Zhang, S., Li, Y., 2015. Image segmentation using mean shift for extracting croplands from high-resolution remote sensing imagery. Remote Sens. Lett. 6, 952–961. https://doi.org/10.1080/2150704X.2015.1093188

Sun, C., Bian, Y., Zhou, T., Pan, J., 2019. Using of Multi-Source and Multi-Temporal Remote. Remote. Multi-temporal Reg. Subtrop. Agric. 19, 1–23.

Thapa, G., 2010. Smallholder or Family Farming in Transforming Economies of Asia, in: IFAD.

Turker, M., Arikan, M., 2005. Sequential masking classification of multi-temporal Landsat7 ETM+ images for field-based crop mapping in Karacabey, Turkey. Int. J. Remote Sens. 26, 3813–3830. https://doi.org/10.1080/01431160500166391

U.N. Dept. of Economic and Social Affairs, 2017. World population projected to reach 9.8 billion in 2050, and 11.2 billion in 2100 | UN DESA | United Nations Department of Economic and Social Affairs, United Nations Department of Economic and Social Affairs.

UN News Centre, 2015. UN adopts new Global Goals, charting sustainable development for people and planet by 2030 [WWW Document]. United Nations Dep. Econ. Soc. Aff. https://doi.org/10.1080/02513625.2015.1038080

UNCTAD, 2015. Commodities and development report, United nations conference on trade and development. https://doi.org/UNCTAD/SUC/2014/5

Ustuner, M., Sanli, F.B., Abdikan, S., Esetlili, M.T., Kurucu, Y., 2014. Crop type classification using vegetation indices of rapideye imagery. Int. Arch. Photogramm. Remote Sens. Spat. Inf. Sci. - ISPRS Arch. 40, 195–198. https://doi.org/10.5194/isprsarchives-XL-7-195-2014

Valero, S., Morin, D., Inglada, J., Sepulcre, G., Arias, M., Hagolle, O., Dedieu, G., Bontemps, S., Defourny, P., Koetz, B., 2016. Production of a dynamic cropland mask by processing remote sensing image series at high temporal and spatial resolutions. Remote Sens. 8, 1–21. https://doi.org/10.3390/rs8010055

Vuolo, F., Neuwirth, M., Immitzer, M., Atzberger, C., Ng, W.T., 2018. How much does multi-temporal Sentinel-2 data improve crop type classification? Int. J. Appl. Earth Obs. Geoinf. 72, 122–130. https://doi.org/10.1016/j.jag.2018.06.007

Wang, C., Chen, J., Wu, J., Tang, Y., Shi, P., Black, T.A., Zhu, K., 2017. A snow-free vegetation index for improved monitoring of vegetation spring green-up date in deciduous ecosystems. Remote Sens. Environ. 196, 1–12. https://doi.org/10.1016/j.rse.2017.04.031

Wardlow, B.D., Egbert, S.L., 2010. A comparison of MODIS 250-m EVI and NDVI data for crop mapping: A case study for southwest Kansas. Int. J. Remote Sens. 31, 805–830. https://doi.org/10.1080/01431160902897858

Wegner, L., Zwart, G., 2011. Who will feed the world? The production challenge, OXFAM. https://doi.org/10.3362/2046-1887.2011.017

Wood, S.N., 2017. Generalized Additive Models An Introduction with R SECOND EDITION, CRC press. Taylor & Francis Group, LLC. https://doi.org/10.1214/ss/1177013609

Wood, S.N., 2011. Fast stable restricted maximum likelihood and marginal likelihood estimation of semiparametric generalized linear models. J. R. Stat. Soc. Ser. B Stat. Methodol. 73, 3–36. https://doi.org/10.1111/j.1467-9868.2010.00749.x

Wu, K.L., Yang, M.S., 2007. Mean shift-based clustering. Pattern Recognit. 40, 3035–3052. https://doi.org/10.1016/j.patcog.2007.02.006

Xiao, X., Boles, S., Liu, J., Zhuang, D., Frolking, S., Li, C., Salas, W., Moore, B., 2005. Mapping paddy rice agriculture in southern China using multi-temporal MODIS images. Remote Sens. Environ. 95, 480–492. https://doi.org/10.1016/j.rse.2004.12.009

Xie, B., Zhang, H.K., Xue, J., 2019. Deep convolutional neural network for mapping smallholder agriculture using high spatial resolution satellite image. Sensors (Switzerland) 19. https://doi.org/10.3390/s19102398

Xie, Q., Dash, J., Huang, W., Peng, D., Qin, Q., Mortimer, H., Casa, R., Pignatti, S., Laneve, G., Pascucci, S., Dong, Y., Ye, H., 2018. Vegetation Indices Combining the Red and Red-Edge Spectral Information for Leaf Area Index Retrieval. IEEE J. Sel. Top. Appl. Earth Obs. Remote Sens. 11, 1482–1492. https://doi.org/10.1109/JSTARS.2018.2813281

Xu, L., Ming, D., Zhou, W., Bao, H., Chen, Y., Ling, X., 2019. Farmland extraction from high spatial resolution remote sensing images based on stratified scale pre-estimation. Remote Sens. 11. https://doi.org/10.3390/rs11020108

Zhang, J., Wang, R., Xie, C., Xie, J., Fu, K., 2013. An algorithm for segmenting pest from crop pest image with complicated background. J. Comput. Inf. Syst. 9, 3857–3864. https://doi.org/10.12733/jcis5818

Zheng, B., Myint, S.W., Thenkabail, P.S., Aggarwal, R.M., 2015. A support vector machine to identify irrigated crop types using time-series Landsat NDVI data. Int. J. Appl. Earth Obs. Geoinf. 34, 103–112. https://doi.org/10.1016/j.jag.2014.07.002

7. APPENDICES

Table 14: Accuracy assessment results for pixel-based classification based on S2 Classical NDVI

	Corn	Potatoes	Summer barley	Winter barley	Winter wheat	Total	UA (%)
Corn	47	15	0	0	0	62	75.10
Potatoes	93	128	1	0	0	222	57.66
Summer barley	5	0	34	0	21	60	56.67
Winter barley	3	4	9	31	5	52	59.62
Winter wheat	2	3	6	19	24	54	44.44
Total	150	150	50	50	50	450	
PA (%)	31.33	85.33	68	62	48	**OA (%)**	**58.67**

Table 15: Accuracy assessment results for pixel-based classification based on $NDVI_{REA}1$

	Corn	Potatoes	Summer barley	Winter barley	Winter wheat	Total	UA (%)
Corn	108	23	2	0	1	134	80.60
Potatoes	32	118	1	0	0	151	78.15
Summer barley	2	0	25	0	13	40	62.50
Winter barley	3	3	2	46	0	54	85.19
Winter wheat	5	6	20	4	36	71	50.70
Total	150	150	50	50	50	450	
PA (%)	72	78.67	50	92	72	**OA (%)**	**74**

Table 16: Accuracy assessment results for pixel-based classification based on $NDVI_{REA}2$

	Corn	Potatoes	Summer barley	Winter barley	Winter wheat	Total	UA (%)
Corn	55	17	1	0	1	74	74.32
Potatoes	86	127	1	0	0	214	59.35
Summer barley	2	0	30	0	17	49	61.22
Winter barley	3	3	9	31	2	48	64.58
Winter wheat	4	3	9	19	30	65	46.15
Total	150	150	50	50	50	450	
PA (%)	36.67	84.67	60	62	60	**OA (%)**	**60.67**

Table 17: Accuracy assessment results for pixel-based classification based on $NDVIR_{EA}3$

	Corn	Potatoes	Summer barley	Winter barley	Winter wheat	Total	UA (%)
Corn	46	23	2	0	1	72	63.89
Potatoes	93	119	0	0	0	212	56.13
Summer barley	5	0	32	0	18	55	58.18
Winter barley	3	5	9	37	1	55	67.27
Winter wheat	3	3	7	13	30	56	53.57
Total	150	150	50	50	50	450	
PA (%)	30.67	79.33	64	74	60	**OA (%)**	**58.67**

Table 18: Accuracy assessment results for pixel-based classification from $NDVI_{REA}4$

	Corn	Potatoes	Summer barley	Winter barley	Winter wheat	Total	UA (%)
Corn	50	21	2	0	1	74	67.57
Potatoes	91	123	0	0	0	214	57.48
Summer barley	2	0	32	0	18	52	61.54
Winter barley	3	3	9	41	0	56	73.21
Winter wheat	4	3	7	9	31	54	57.41
Total	150	150	50	50	50	450	
PA(%)	33.33	82	64	82	62	**OA (%)**	**61.56**

Table 19: Accuracy assessment results for pixel-based classification using NDVIren1

	Corn	Potatoes	Summer barley	Winter barley	Winter wheat	Total	UA(%)
Corn	51	31	4	0	5	91	56.04
Potatoes	98	118	9	1	0	226	52.21
Summer barley	0	1	28	0	18	47	59.57
Winter barley	1	0	2	39	2	44	88.64
Winter wheat	0	0	7	10	25	42	59.52
Total	150	150	50	50	50	450	
PA(%)	34.00	78.67	56.00	78.00	50.00	**OA(%)**	**58.00**

Table 20: Accuracy assessment results for pixel-based classification using NDVIren3

	Corn	Potatoes	Summer barley	Winter barley	Winter wheat	Total	UA (%)
Corn	40	21	2	0	4	67	59.70

Potatoes	104	119	6	2	0	231	51.52
Summer barley	0	1	24	0	15	40	60.00
Winter barley	3	8	6	38	0	55	69.09
Winter wheat	3	1	12	10	31	57	54.39
Total	150	150	50	50	50	450	
PA (%)	26.67	79.33	48.00	76.00	62.00	**OA (%)**	**56.00**

Table 21: Accuracy assessment results for pixel-based classification using NDVIren2

	Corn	**Potatoes**	**Summer barley**	**Winter barley**	**Winter wheat**	**Total**	**UA (%)**
Corn	71	38	21	23	4	157	45.22
Potatoes	27	81	10	0	14	132	61.36
Summer barley	3	2	12	1	7	25	48.00
Winter barley	49	25	7	26	12	119	21.85
Winter wheat	0	4	0	0	13	17	76.47
Total	150	150	50	50	50	450	
PA (%)	47.33	54.00	24.00	52.00	26.00	**OA (%)**	**45.11**

Table 22: Accuracy assessment results for pixel-based classification using NDVIre1

	Corn	**Potatoes**	**Summer barley**	**Winter barley**	**Winter wheat**	**Total**	**UA (%)**
Corn	47	16	4	1	1	69	68.12
Potatoes	102	131	9	0	2	244	53.69
Summer barley	0	3	27	0	18	48	56.25
Winter barley	1	0	2	27	11	41	65.85
Winter wheat	0	0	8	22	18	48	37.50
Total	150	150	50	50	50	450	
PA (%)	31.33	87.33	54.00	54.00	36.00	**OA (%)**	**55.56**

Table 23: Accuracy assessment results for pixel-based classification using NDVIre2

	Corn	**Potatoes**	**Summer barley**	**Winter barley**	**Winter wheat**	**Total**	**UA (%)**

Corn	88	57	21	14	6	186	47.31
Potatoes	41	83	12	7	7	150	55.33
Summer barley	8	4	16	1	8	37	43.24
Winter barley	12	5	0	14	2	33	42.42
Winter wheat	1	1	1	14	27	44	61.36
Total	150	150	50	50	50	450	
PA (%)	58.67	55.33	32.00	28.00	54.00	**OA (%)**	**50.67**

Table 24: Accuracy assessment results for pixel-based classification using NDVIre3

	Corn	**Potatoes**	**Summer barley**	**Winter barley**	**Winter wheat**	**Total**	**UA (%)**
Corn	52	40	16	5	2	115	45.22
Potatoes	22	34	3	0	2	61	55.74
Summer barley	46	40	21	16	18	141	14.89
Winter barley	9	11	3	15	4	42	35.71
Winter wheat	21	25	7	14	24	91	26.37
Total	150	150	50	50	50	450	
PA (%)	34.67	22.67	42.00	30.00	48.00	**OA (%)**	**32.44**

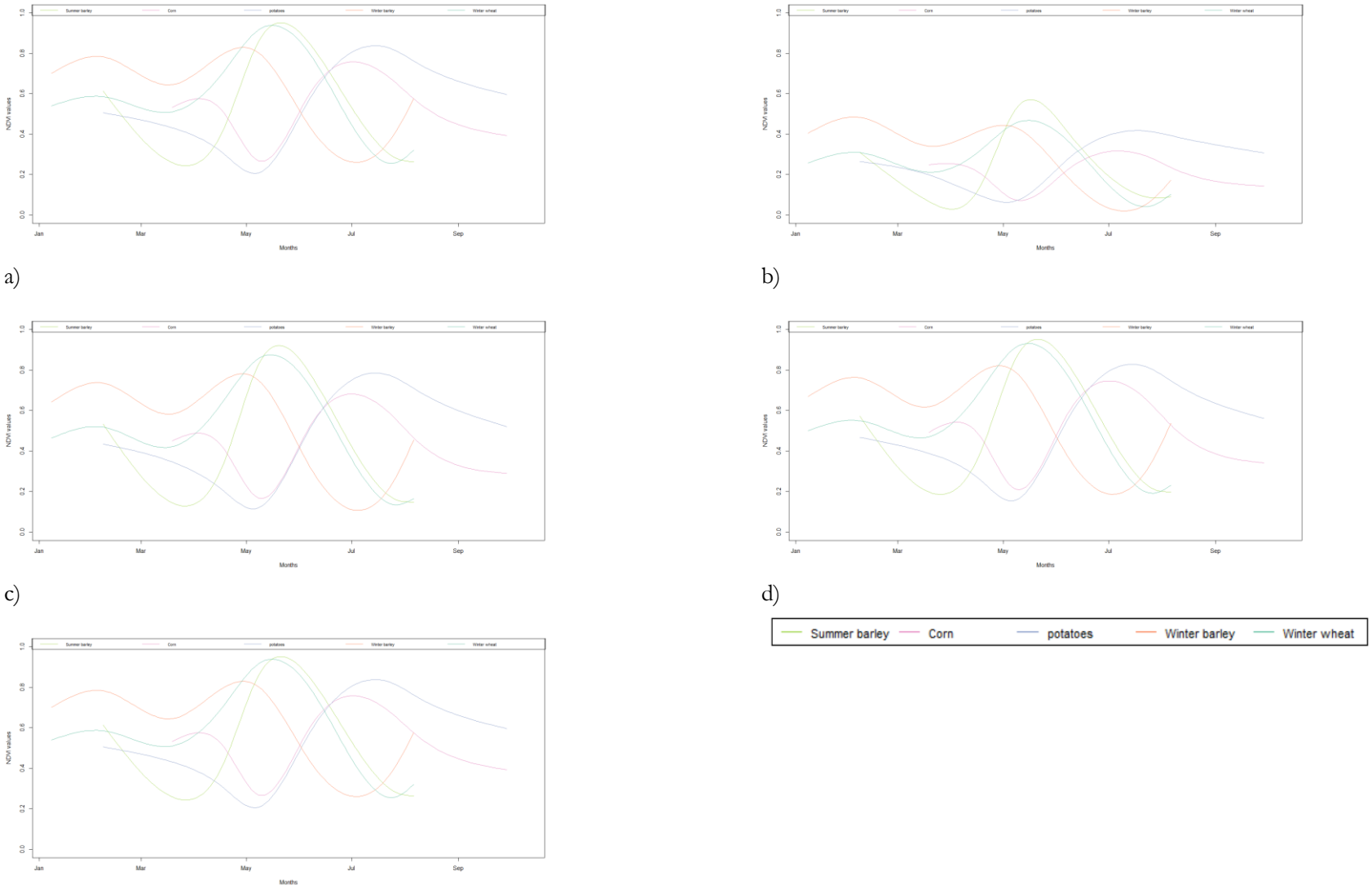

Figure 12: Temporal profiles generated a) using classical NDVI and $NDVI_{REA}$ for b) $NDVI_{REA}1$, c) $NDVI_{REA}2$, d) $NDVI_{REA}3$ and e) $NDVI_{REA}4$ from S2 images

Mapping crops in smallholder farm systems from high-spatial-resolution and multi-temporal satellite images